CHALMERS
UNIVERSITY OF TECHNOLOGY

Recycling of CIGS flexible solar cells: Investigation of organic acids leaching

Master's thesis in Innovative and Sustainable Chemical Engineering

PARTH SOMANI & HANXIANG LIANG

DEPARTMENT OF CHEMISTRY AND CHEMICAL ENGINEERING
CHALMERS UNIVERSITY OF TECHNOLOGY
Gothenburg, Sweden 2023
www.chalmers.se

Master's thesis 2023

Recycling of CIGS flexible solar cells: Investigation of organic acids leaching

Parth Somani & Hanxiang Liang

CHALMERS
UNIVERSITY OF TECHNOLOGY

Department of Chemistry and Chemical Engineering
Industrial Material Recycling
Chalmers University of Technology
Gothenburg, Sweden 2023

Recycling of CIGS flexible solar cells: Investigation of organic acids leaching
Parth Somani & Hanxiang Liang

Supervisor: Burçak Ebin,Inudstrial Materials Recycling
Examiner: Martina Petranikova,Industrial Materials Recycling

Master's Thesis 2023
Department of Chemistry and Chemical Engineering
Industrial Material Recycling
Chalmers University of Technology
SE-412 96 Gothenburg
Telephone +46 31 772 1000

Cover: Flexible solar cells.

Typeset in LaTeX
Printed by Chalmers Reproservice
Gothenburg, Sweden 2023

Recycling of CIGS flexible solar cells: Investigation of organic acids leaching
Parth Somani
Hanxiang Liang
Department of Chemistry and Chemical Engineering
Chalmers University of Technology

Abstract

The Photovoltaic market has been rising sharply in recent years and is expected to grow steadily in the upcoming years. The copper-indium-gallium diselenide (CIGS) solar cell has become a more and more significant role in the photovoltaic industry, and its application in the second generation of solar cells has increased in recent years, which means photovoltaic waste will be prominent in the future. To reduce resource consumption and recycle valuable materials from an economical and environmental perspective, further research on metal recovery should be carried out. Currently, from an economic point of view, recycling CIGS solar cells is not feasible on an industrial scale, and research is limited. The current end-of-life module recycling is done using thermal decomposition, pyrolysis treatment, and dry etching in the presence of Chlorine gas at high temperatures, which could require high energy demand and high effort for the purification of metals. Moreover, due to the drawbacks of inorganic acid leaching, such as toxic gas production and low selectivity of the metals. The viability of organic acids as an alternative leaching agent needs to be investigated. The project aims to extract the valuable metals present in CIGS solar cells by comprehending the influence of leaching variables through utilizing organic acids in an environmentally friendly way. Citric acid and tartaric acid were employed for the leaching process, as well as nitric acid leaching was studied to compare the results. Some leaching conditions such as concentration, surface area to liquid ratio, temperature, and agitation method are considered to find the optimum condition for the metal recovery from CIGS solar cells. The results show that different division methods have an impact on extracting silver with nitric acid. The mass of silver in the whole solar cell is 44% more than in the divided cell sample. For 1M citric acid with a surface area to liquid ratio of 1:3 cm^2/ml, temperature of $50°C$ and 100 rpm stirring speed, a high selectivity of Zn and In at 8 hours was observed.

Keywords: Recycling, acid leaching, CIGS solar cells,PV

Acknowledgements

I want to thank my supervisor Burcak Ebin and our ex-supervisor Ioanna Teknetzi, for their continuous support and guidance during this thesis project.

I would like to extend my thanks to all the PhD students and the researchers in the Department of Industrial Material Recycling and Nuclear Chemistry for your help throughout our time of thesis project.

At last, I would like to thank Martina Petranikova for accepting the request to be our examiner and taking the time to go through our report.

Hanxiang Liang, Gothenburg, June 2023
Parth Somani, Gothenburg, June 2023

List of Acronyms

Below is the list of acronyms that have been used throughout this thesis listed in alphabetical order:

CIGS	Copper Indium Gallium Selenide
PV	Photovoltaic
ICP-OES	Inductively Coupled Plasma Optical Emission Spectroscopy
EVA	Ethyl vinyl acetate
PVF	Polyvinyl fluoride
D2EHPA	Di-(2-Ethyl Hexyl) phosphoric acid
SEM-EDS	Scanning Electron Microscope-Energy-Dispersive X-Ray
XRD	X-Ray Diffraction

Contents

List of Figures

List of Tables

1
Introduction

1.1 Overview of PV technology

According to the Intergovernmental Panel on Climate Change (IPCC), a goal has been set to keep the warming under $2°C$ and pursue an even lower warming cap of $1.5°C$. The International Energy Agency reported that the path to net-zero emission by 2050 hinges on an unprecedented push for renewable energy technologies. Due to the deterioration of the environment and the energy crisis, there has been a pressing need to develop environmentally friendly and renewable energy technologies. Solar Photovoltaics(PV) or Solar cells are considered a promising energy-generating technology as they can generate electricity directly from the sun, reducing our reliance on fossil-based energy and greenhouse gas emissions. Currently, solar energy technology stands at third for the most used renewable source in the world after hydro and wind power, which occupy the first and second position[6]. According to data shown in figure 1.1, the global PV deployment is expected to grow in an ascending manner, reaching 1,632 GW in 2030, and with an annual growth rate of about 2.5% it could reach about 4500 GW of global PV capacity by 2050[1].

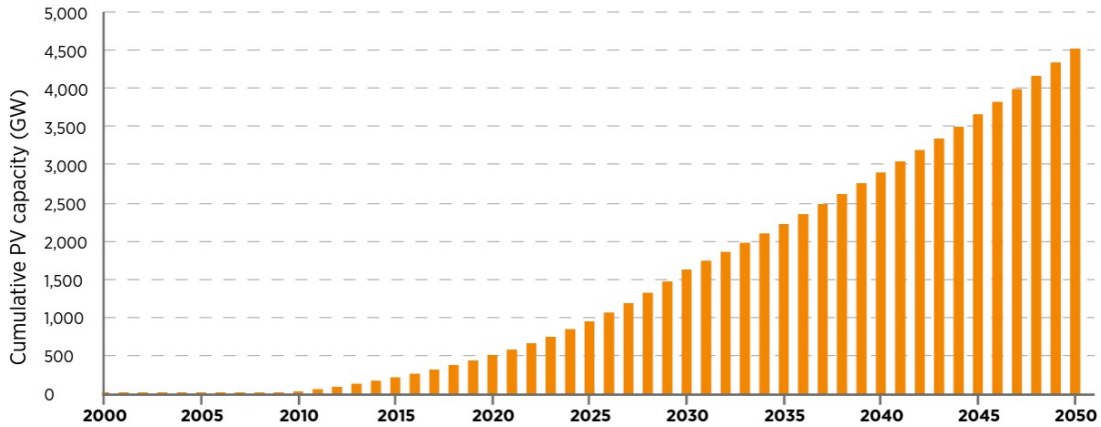

Figure 1.1: Projected cumulative global PV capacity[1].

In recent years, photovoltaic has been the fastest-growing technology by capacity additions in renewable power generation. In 2021, photovoltaics cover 3.5% of worldwide gross electricity generation and exceeded 1000 TWh of power generation by marking 22% growth(179 TWh) from 2020[7]. Even though the production and installation of PV modules are on the rise, the number of end-of-life PV modules

is relatively small. Therefore, while manufacturing and utilizing PV, a cumulative PV panel waste is predicted to be around 78 million tons by 2050[8]. Currently, the European Union (EU) leads the way in regulating end-of-life PV modules under the Waste Electrical and Electronic Equipment Directive (WEEE). PV panels are not allocated a distinct category under the WEEE directive. They are instead categorized with consumer equipment in category 4, posing challenges in tracing and monitoring the actual behavior of PV panel flows [9].

At present, there is a lack of industrial-scale end-of-life treatment (EoLT) options for photovoltaic products. Recycling of these products is currently limited, particularly in the case of photovoltaic systems. The technical and economic challenges involved are significant PV modules usually have a lifespan of 20-30 years.

2
Background

2.1 Photovoltaics cell types

PV cell technologies are classified into three generations, depending on the basic material used and their level of commercial maturity: 1. First-generation PV systems: These use wafer-based crystalline silicon(c-Si) technology, monocrystalline or multi-crystalline silicon. 2. Second-generation PV systems: These are based on thin-film PV technologies and generally include three main families: 1) amorphous (a-Si) 2) CadiumTelluride (CdTe); and 3) Copper-Indium-Selenide (CIS) and Copper-Indium-Gallium-Diselenide (CIGS). These are called thin films because the semiconducting materials used for the production of the cell are only a few micrometers thick. These technologies are being deployed on a commercial scale, but some at low volumes. 3. Third-generation PV systems: These are the cell technologies that are currently in the demonstration phase or still under development. These cells aim to improve upon the efficiency and cost-effectiveness of previous generations of solar cells by utilizing novel concepts and materials. They also include solar cells sensitized by dye, tandems, and perovskite-sensitized solar cells[10]. The conventional silicon-wafer-based solar module's shares of production are 95% of the total PV market and CIGS production shares reach 1.2%. It is obvious that c-Si production takes up the majority of the shares, but CIGS solar cell shows a high efficiency of 23.4% compared to CdTe of 21.0% and less material usage is required since the CIGS thickness is lower than c-Si wafer[11, 12]. In this study, one cell type is investigated, the CIGS solar cells.

2.1.1 CIGS Solar Cells

CIGS belongs to the family of I-III-VI2 semiconductor materials that crystallize in a tetragonal chalcopyrite structure (Fig 2.1) and its chemical form is expressed as $Cu(In_x, Ga_{1-x})Se_2$ where the value of x can differ between 0 (pure copper gallium selenide) and 1(pure copper indium selenide). The CIGS thin film solar cell is a second-generation solar cell with high conversion efficiency, low-temperature coefficient, and strong light absorption capability [13]. As a result of these advantages, the energy payback for CIGS solar cells is much shorter compared to conventional crystalline silicon solar cells. The flexible characteristic of the CIGS solar cells makes them suitable for applications on roofs, transport vehicles, and buildings.

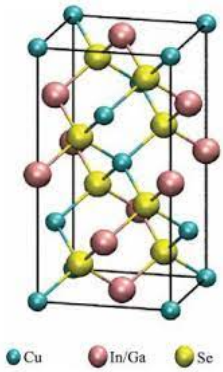

Figure 2.1: The crystal structure of the CIGS light-absorbing layer [2].

Developing the CIGS solar cell is necessary as well. Nowadays, the common ways to synthesize the CIGS solar cell are selenization[14], electrodeposition, chemical spray pyrolysis[15], paste coating[16] and so on. In the manufacturing process, the utilization rate of raw materials, like indium, is relatively low[17]. Simultaneously, the life span of the CIGS thin film solar cell is around 25 years, and the CIGS solar cell waste is predicted to peak at 45000 tons in 2035[18, 19].

Normally the whole structure has a thickness of around 3 μm - 4μm. The structure of a CIGS solar cell is made of seven layers in the sequence, could be seen in Figure2.2: 1. the metal grid contact layer with Ni/Al(2μm) 2. the transparent conducting oxide layer is normally consisted of ZnO/Al(0.5-1.5μm) or IndiumTin Oxide(ITO) 3. n-type CdS window layer(40-80nm) 4. ZnO buffer layer($\sim$400nm) 5. p-type CIGS absorber layer(1-3μm) 6. molybdenum back contact layer(0.5-2μm) 7. a glass substrate[12, 20]. The function of the CIGS solar cell is that the light goes through the Transparent Conductive Oxide(TCO) and buffer layer, and the CIGS absorbs it not only from the TCO, but also the reflected light from Mo back contact[21]. In order to obtain a desirable energy band gap range of 1.06-1.7 eV for CIGS solar cells, it is imperative to adjust the Ga/(Ga+In) ratio.

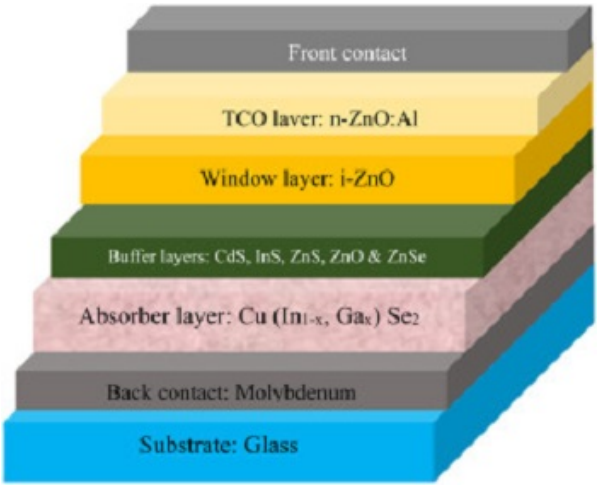

Figure 2.2: The structure of CIGS solar cell layer.

The CIGS absorber layer comprises a thin film of $Cu(In, Ga)Se_2$ [22]. The CIGS solar cell absorption layer comprises four elements: Cu, In, Ga, and Se. These four valuable metals exist as mixed selenides in the CIGS solar cells. Global selenium resources are low and mostly linked with sulfide minerals. The industrial-level grade of Se is mainly extracted from the copper anode slime[23]. High-purity Se is a critical material due to its important role in metallurgy, semiconductors, and others. These critical materials (In & Ga) are meagerly found on Earth and are hard to extract. In and Ga are mainly processed as a by-product from the hydrometallurgical Zn industry and the aluminum extraction industry. In the current status, the short-term CIGS PV technologies show the indium consumption of 14 tons per gigawatt without thickness reduction, and In cost contributes 7% of the CIGS solar cell at a price 500 dollars per kilogram[24].

Therefore, it is important to take certain steps to recycle CIGS solar cells in order to retrieve valuable metals and process them using an environmentally friendly recycling method.

2.2 End-of-Life PV module recycling

Among all the thin-film PV technologies, the CIGS-based technology has become the fastest-growing due to its potential for low cost and high performance. As mentioned earlier, the PV cumulative waste is gonna reach 78 million tons by 2050. Currently, the recovery of materials from end-of-life products is hardly present because their recycling is technically and economically challenging[25]. Some existing PV recycling pathways must be studied to understand their importance from both technological and economic perspectives.

FirstSolar has developed a recycling process for the end-of-life CdTe(Cadmium Telluride) modules. The recycling process occurs as follows[26, 27]: the modules are breakdown into pieces small enough to break lamination bonds between layers. Then, the semiconductor layers are extracted by the leaching process using acid and hydrogen peroxide in a slowly rotating, stainless steel drum. The remaining amount in the drum is then passed through a classifier which segregates the solid (including glass and laminate materials) from the metal-rich liquid. A vibrating screen separates the glass from the larger pieces of laminate material. The glass is cleaned to remove residual semiconductor material and then packaged for recycling. Meanwhile, the metal-rich liquid is pumped to the precipitation unit, and three stages of precipitate are carried out by increasing the pH value to collect the concentrate in a thickening tank. ANTEC Solar GmbH developed a recycling method for CdTe modules and designed a pilot plant with a similar approach to the previous method. In this process, the first step is the physical disintegration of modules into fragments. The pyrolysis of module fragments removes EVA (ethylene vinyl acetate) in an oxygen-rich atmosphere at a temperature of at least $300°C$. At last, at a temperature of more than $400°C$, the etching process of module components is done in the presence of the chlorine gas in the atmosphere resulting in the production of $CdCl_2$ and $TeCl_4$. The generated $CdCl_2$ and $TeCl_4$ are then condensed

and precipitated by cooling and later refined to recover the metal[28]. As it can be understood from the two recycling processes (FirstSolar and Antec Solar GmbH) that after chemical processes disposal of waste liquids is essential, use of an environmentally friendly solvent and reduction in the amount applied is also necessary to improve the process efficiency [29].

The optical approach used by Loser Chemie stands out as a distinctive option when compared to the conventional methods. The company has patented a new way to recycle solar panels using mechanical and chemical methods. To begin with, the implementation of optical technologies simplifies the process of separating the glass panels and sandwich structures without causing any damage to the glass. After the optical treatment, the cover glass and substrate glass (with compound layers) are separated. The leaching of the compound layers is done using alkane sulfonic acids(such as methane sulfonic acids). After this, the metals can be obtained as individual metal compounds and then recycled and purified by a metal refinery company[29].

To evaluate the economic feasibility of recycling solar modules, McDonald et al.[5] compared the landfill disposal cost and total profitability of recycling for five different types of PV material-based solar cells.

Table 2.1: Landfill disposal cost of PV modules and total profitability of recycling [5].

	CIGS	CdTe	c-Si	p-Si	a-Si
E(W/m^2)	100^a	108^a	144^a	138^a	90^a
Weight(kg)	28^b	12^c	15.4^d	19.4^e	19.1^f
Nominal power(W)	160^b	77.5^c	180^d	230^e	128^f
W(kg/module)	17.5^b	16.72^c	12.32^d	11.64^e	13.43^f
Tipping cost($/kg)	0.05^g	0.39^g	0.05^g	0.05^g	0.05^g
Disposal cost($)	0.87	6.45	0.61	0.58	0.67
Total profitability($) P_T= P_t+D-C	22.25	-0.24	-23.96	-23.99	0.73-C

In the table 2.1, E: power per unit area of the individual module(W/m^2), W: total waste mass per module(kg/module), T: tipping cost($/kg), D: final disposal cost($), C: cost of recycling($/module) and P_T: total profit from recycling($). The higher profitability of recycling CIGS solar cells is attributed to the valuable presence of rare metals like In and Ga, as well as other precious metals. At the same time, we can observe that the landfill disposal cost is comparatively much lower than the recycling cost of PV modules.

Furthermore, technological innovation will also be required to develop technologies that allow for the recycling of all useful semiconductor materials at high rates and very little cost. Also, create policies that help to ensure the investment required to recapture the critical materials from PV modules.

2.3 Recycling methods of CIGS solar cell

The retrieval of metals like In, which are both expensive and scarce, along with valuable metals like Se and Ga present in the CIGS absorber layer, can be achieved through the utilization of processes such as hydrometallurgy[30], pyrometallurgy, and comprehensive treatments[31]. Through science and technology, we can effectively manage our limited resources and make the most of them in a sustainable manner. Most of these processes are not yet applied on an industrial scale due to the high concentration of the leaching solutions and their contamination.

Theocharis et al. [32] conducted the experiment, which started with the thermal treatment where the solar cell was heated up to $1500°C$ to decompose the element. EVA and PVF membranes were dismantled at $540°C$ to $550°C$. Then, followed by a hydrometallurgy treatment, the separated glass fragments were leached with HNO_3 solution to recovery In, Ga, Cu, Mo, Zn. Diluted D2EHPA in kerosene was used to separate In and Ga by solvent extraction, 97% of In was selectively separated without Ga co-extraction at pH=1.5.

Marwede et al. [33] explored proven recycling concepts for thin-film solar cells, specifically copper indium gallium selenide (CIGS) solar cells. Recycling of CIGS modules involves three main steps: separating the modules, removing the coating from the substrate, and collecting and refining the metals and semiconductors.

Alessia et al. [34] tested different leaching agents, including H_2SO_4, HNO_3, HCl, citric acid and $NaOH$, in the presence of mobilizing agents such H_2O_2 or glucose for recovery of In and Ga from end-of-life CIGS PV panels.The combination of citric acid and H_2O_2 at $80°C$ for 1 hour resulted in over 90% efficiency, making it the most effective leaching combination among those tested.

Besides, Gustafsson et al. [22] also went through a pyrometallurgical process to heat the CIGS powder obtained from the CIGS solar cell module with the flow of nitrogen gas and oxygen gas at $600°C$. The CIGS material was oxidized to selenium dioxide and other metal oxides. When the selenium dioxide was cooled down to crystal form, it was dissolved in the mixture of glacial acetic acid and deoxybenzoin and reduced with sulfur oxide to the solid form. The different metal oxides were formed during the oxidation reaction; they mainly consist of oxides of indium and copper. Indium was separated by 7M NaOH solution and copper was by water leaching[35].

It can be inferred from the preceding section that while recycling technologies for silicon-based photovoltaic (PV) modules and related manufacturing waste have been extensively investigated, the recycling of thin-film solar cells is still in its developmental phase. Nevertheless, aside from the technological factors, there are still some critical issues related to the establishment of PV product recycling systems, among which the environmental benefits and economic viability are very important.

3

Theory

In the following section, a basic overview of the things required are mentioned to understand the basic concepts of leaching and the analysis instruments throughout this project.

3.1 Leaching

Hydrometallurgy processes have an edge over pyrometallurgical processes because it's eco-friendly and economical for low-grade metals reserves[36]. Hydrometallurgical approaches have three stages: metal dissolution, concentration and purification, and metal recovery. Acid leaching is the most often used in hydrometallurgical technology.

Leaching is an extraction method used in hydrometallurgical processing by which metals of interest are dissolute from the solid phase into the aqueous solution. Precipitation and solvents extraction can be used to separate precious components from polymetallic leachate.

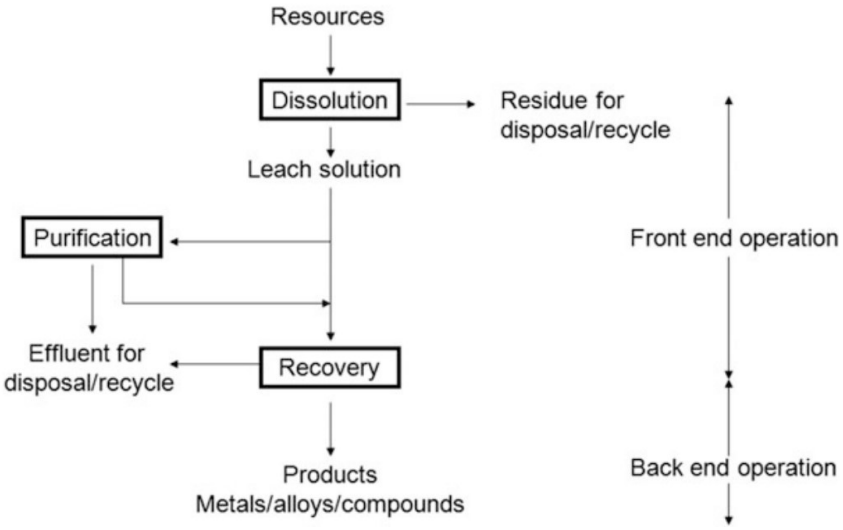

Figure 3.1: Basic unit processes in hydrometallurgy[3].

The leaching process is affected by several factors, each of which plays a significant

role in determining the leaching rate. These factors include the concentration of the leaching agent, the temperature at which the process is carried out, the speed of agitation, and the ratio of surface area to liquid. Any variation in these factors can affect the leaching rate, and it is therefore crucial to carefully control and optimize each parameter to achieve the desired results. In this context, surface area refers to the sample's surface area, and liquid means the volume of the leaching agent (in ml).

3.2 Analysis Instruments

The analysis method used in this project was inductively coupled plasma optical emissions spectroscopy, scanning electron microscopy, and x-ray diffraction. The basic principle of the instruments used will be covered in this section.

3.2.1 Inductively Coupled Plasma-Optical Emissions Spectroscopy

Inductively coupled plasma optical emission spectroscopy (ICP-OES) is the technique used for several applications that require quantifying the elemental content of a sample.

The basic principle of inductively coupled plasma optical emissions spectroscopy depends upon the spontaneous emissions of photons generated from the atoms or ions, and these ions and atoms are excited by a radio frequency discharge.[37]

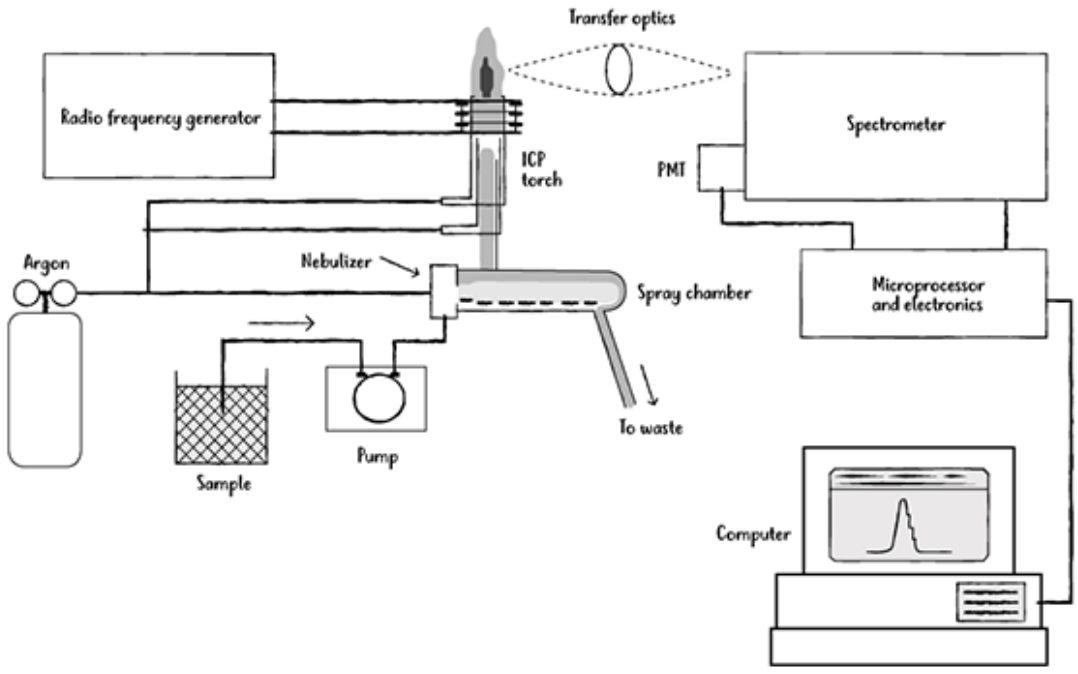

Figure 3.2: Instrumentation of ICP-OES.

The ICP-OES instrument consists of nebulizers, spray chamber, a sample injector, ICP torch, RF generator, a spectrometer, emissions detectors, signal processing, and software.

In the ICP-OES instrument, the liquid samples are pumped into the nebulizer with the help of the peristaltic pump. In the nebulizer, the injected liquid samples are transformed into the form of an aerosol or mist through a process known as the aerosol nebulization process. After the aerosol formation, the mist enters the plasma at high temperatures, sufficient to break down the sample into atoms and provide the energy for ionization and excitation. In the spray chamber, the nebulized sample is fed to the plasma discharge from the nebulizer to the ICP torch. In the ICP torch, the chamber sends argon gases between the inner and outer flow to maintain the plasma discharge and to ease the introduction of an aerosol sample into the plasma. Using the ionized plasma, the aerosol sample is atomized and get excited to a higher energy state. When the excited atoms fall back to the ground energy state, they emit light at a characteristic wavelength which is measured using an optical spectrometer[38]. The signals from multiple elements could overlap, and to mitigate this issue, the wavelength corresponding to each element is separated via an optical grating device so that each element can be individually detected. The intensity measured in the detector is proportional to the concentration offset element in the analyte. At last, the Thermo Scientific^{TM} Intelligent Data Solution Software which acquires the measured intensities and processes data through a predefined calibration to produce elemental concentrations.

The plasma view is of two types: axial view and radial view. In axial configuration, the plasma is viewed head-on and is useful for detecting elements present at low concentrations, whereas in radial configuration, the plasma is viewed from the side and has better detection limits for elements present at high concentrations.

3.2.2 Scanning Electron Microscope

Scanning electron microscopy (SEM) is an instrumental method that provides high-resolution magnified images of a sample's surface topography using a focused beam of electrons. The signals used to produce an image are a result of the interaction of the beam of electrons with the atoms on the surface and within the sample. They are divided into secondary electrons, backscattered electrons and x-rays to give information about the sample's morphology. It can create a magnification image resolution of nearly 10 nm.

In addition to high-resolution imaging, Energy-Dispersive X-Ray(EDX) Spectroscopy is used to run an elemental analysis of the surface of a sample with an SEM. In EDX, when the sample is exposed to the electron beam, each element creates a unique set of peaks on the emissions spectrums(characteristics x-rays from the specimen), which helps characterize each element in the sample.

3.2.3 X-Ray Diffraction

X-ray diffraction(XRD) is a technique that determines a sample's composition or crystalline structure. X-rays are created when electrons extracted from the filament(Tungsten) and accelerated by high voltage bombard a target.Cu is commonly used for the target material. An X-rays has a wavelength of 0.01 to 10 nanometers, with a frequency of 3×10^{16} Hz to 3×10^{19} Hz. XRD method can be applied to know the wide variety of information about the fine-scale structure of matter. It possesses enough energy to ionize atoms, known as ionization energy.

XRD is based on Bragg's law: The reflected X-rays from different crystal layers with long-range order undergo constructive interference.

$$2dsin\theta = n\lambda \tag{3.1}$$

where d is lattice spacing, θ is angle between the wavevector of the incident plane wave, k_o, and the lattice planes, λ is the wavelength and n is an integer, the order of the reflection[39].

X-ray diffraction is based on the constructive interference of monochromatic x-rays and a crystalline sample.

These X-rays are collimated and directed onto the sample. As the sample and detector are rotated to satisfy Braggs equation, the intensity of the reflected X-rays is recorded. When the geometry of the incident X-rays impinging the sample satisfies the Bragg Equation 3.1, constructive interference occurs, and a peak in intensity occur. A detector records and processes this X-ray signal and converts the signal to a count rate which is then output to a device such as a printer or a computer monitor.

The data obtained from the XRD was compared with the standardized XRD data(International Centre for Diffraction Data) to identify which composite of the metal is formed.

4

Materials and Methods

4.1 Sample preparation

All the CIGS solar cells are provided by Midsummer AB company. The experimental water is distilled water and the reagents are of analytical grade. The whole solar cell is observed as an approximate square with a round edge in the corner and three silver lines distributed on the top surface. Two different cell division methods were used to cut the solar cell. In 4.1b, we cut the solar cells into four equal parts, while cut it into sixteen $2.3 \times 5\ cm^2$ rectangles, and some areas remain in the corner in4.1c.

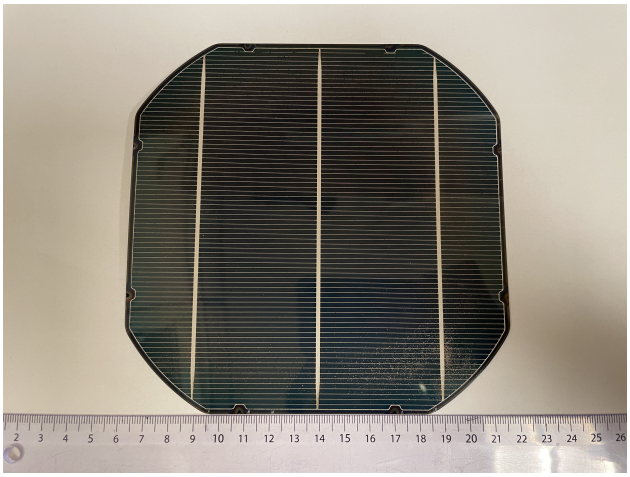

(a) Example of the $15.6 \times 15.6\text{cm}^2$ solar cell

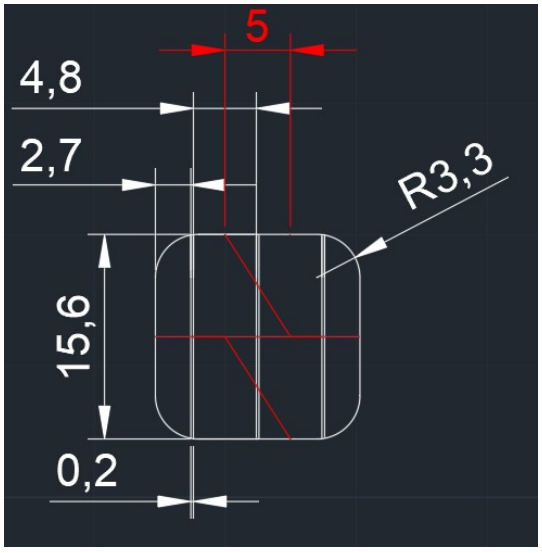

(b) Design of solar cell division to cut four equal pieces

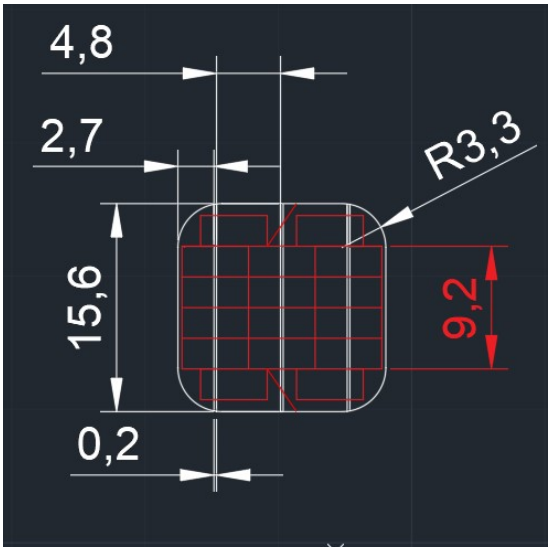

(c) Design of solar cell division to cut $2.3 \times 5\text{cm}^2$ rectangle

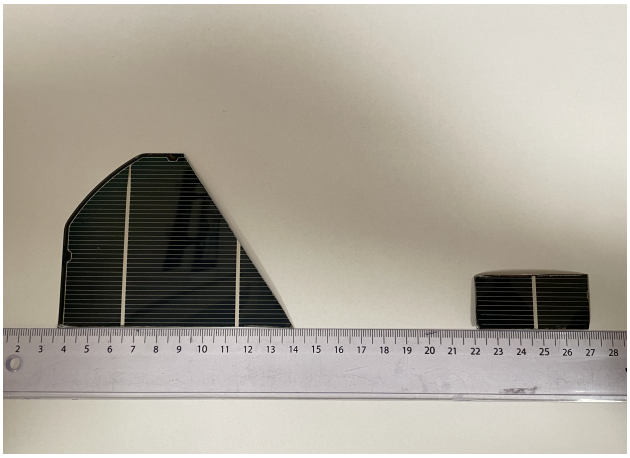

(d) Plot of big sample and small sample

Figure 4.1: Example of two different solar cell division methods.

4.2 Chemicals

The chemicals used in the experiments are of ACS reagent grade. All acids were supplied from SIGMA- ALDRICH®, except for nitric acid (69%), which was provided from Emsure®. The leaching experiments were carried out using different inorganic and organic acids: nitric acid (HNO_3), citric- acid ($C_6H_8O_7$), and tartaric acid ($C_4H_6O_6$). The acid solutions were prepared by diluting the concentrated acids and dissolution of the organic acid powder with the appropriate amount of Mili-Q water (18.2 MΩ cm at 25 ± 2°C).

4.3 Digestion and Leaching process

The leaching of the whole solar cell was carried out on an orbital shaker with 8M nitric acid solutions and different concentrations of citric acid solutions in a closed PP plastic container using different solar cell divisions. The volume of the leaching solution depended on the surface area to liquid ratio. The experiments took place at room temperature at 100 rpm on the orbital shaker. For the kinetics study, the samples were leached for 1, 2, 4, 6, 8, 24, and 28 hours respectively. At the sampling time, 0.3ml of the samples were taken by syringe and filtered through a 0.45μm filter to remove any solid residues in the syringe. For the reaction that took place at room temperature, the pH values of the acids at each time interval from 1 hour to 28 hours whereas for high temperatures values, the pH values of the acids before leaching and leachates after 24 hours were measured using MeterLab^{TM} PHM 240 pH/ion Meter pH electrode calibrated using Radiometer analytical pH buffers at pH of 2, 4 and 7. The same calibration methods was used in all other pH measurements. The unknown samples from 8M nitric acid solution were diluted in 0.5M nitric acid solution with a dilute factor of 10 for elemental-composition analysis. In comparison, the samples from the citric acid solution were diluted in 0.5M nitric acid and yttrium solution with the same dilute factor. The glasses have been soaked in 4M nitric acid for a minimum of 24 hours before use, followed by thorough rinsing with Mili-Q water.

Figure 4.2: Acid leaching with inorganic acid and organic acid on orbital shaker.

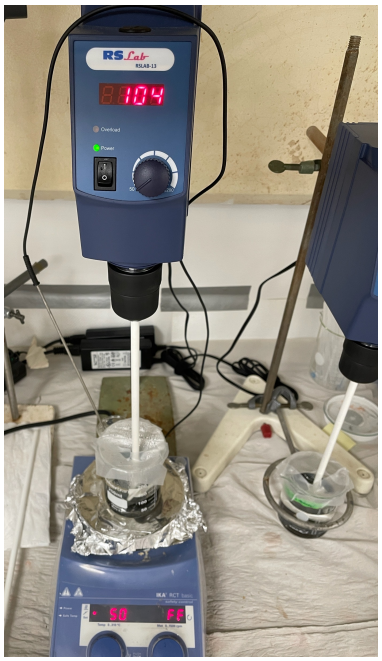

Figure 4.3: Acid leaching with citric acid by using stirrer machine and hot plate.

The experimental setup was amended to study the effect of the temperature on the leaching. The leaching was performed in a beaker equipped with a mechanical stirrer, and a hot plate connected with a thermocouple was used to control the desired temperature. After the experiments were completed, the pieces of the solar cells were immersed in Milli Q water for approximately 3 seconds, then removed from the water and left to air dry. It was only after it had been determined that there would be a need to do so that the analysis of the sample surface was done. All the measurements were performed in triplicate samples (each sample used from different solar cells), and the results were presented as the mean values ± standard deviation.

4.4 Sample analysis

Inductively Coupled Plasma – Optical Emission Spectroscopy (Thermo iCAP 6500) was used to analyze the concentration of metal elements in the solutions. The calibration curve for elements in ICP-OES was based on five standard solutions with concentrations of 2.5ppm, 5ppm, 10ppm, 20ppm, and 40ppm. The specific volume of 1000ppm metal solution was added to prepare to mother liquid solution and diluted with 0.5M HNO_3. Then collected the solution from the mother liquid was used to prepare the different standard solutions.

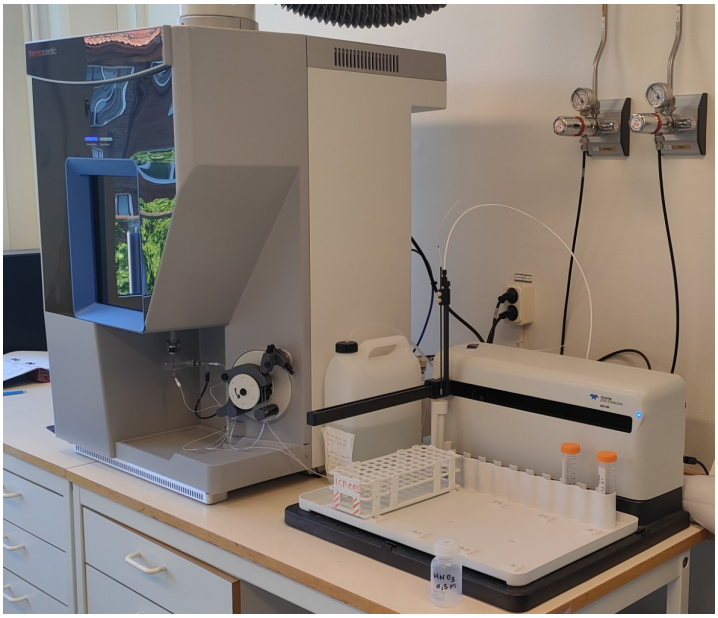

Figure 4.4: ICP-OES machine.

The sensitivity of the methods was identified using the limit of detection(LOD) value. The smallest quantity of analyte that is "significantly different" from a blank. The detection limit was taken as the mean signal for blanks plus 3 times the standard deviation of a low-concentration sample[40]. For each analyte, a 1 ppm Internal Standard 'Y' (Yttrium) has been applied. To ensure accurate and dependable outcomes during analyses, the sample, blank, and calibration standards were treated with the addition of the internal standard. This compensates for both systematic and random error, resulting in reliable results. To study the precipate formed during leaching, it was separated from by centrifugation and to understand the morphology of the residue, SEM-EDS was employed. In our case, Backscattered Electrons images was acquired using beam acceleration voltages of 10kV and 20kV. At last, The chemical composition of the precipitate found in the leaching solutions was further verified using XRD Bruker D8 Advance (Bruker Corporation, Billerica, MA, USA) with Cu K_α used to examine the phase content.

4.5 Calculation of mass of metals

The concentration of each element was obtained from the ICP-OES. The surface area of the solar cell is 233.8 cm^2.To calculate the mass of the element per solar cell, the equations 4.1, 4.2, 4.3 are used:

$$M(whole) = C \times V \times Df \times 0.001 \tag{4.1}$$

$$M(big) = C \times V \times Df \div 58.45 \times 233.8 \times 0.001 \tag{4.2}$$

$$M(small) = C \times V \times Df \div 11.5 \times 233.8 \times 0.001 \tag{4.3}$$

where,
M = mass of the element per solar cell (mg);
C = concentration of element from ICP-OES(ppm);
V = volume of the leaching solution (ml);
Df = dilute factor.

5

Results and Discussion

5.1 Inorgaric acid leaching

The leaching process uses inorganic acid in extractive metallurgy due to its relatively low cost. Indium Tin Oxide (ITO) comprises different oxides of In and Sn, while the SnO_2, and In_2O_3 are the main contents. During acid leaching, the chemical reactions that might take place are as follows:[35, 41]

$$In_2O_3 + 6H^+ \rightarrow 2In^{3+} + 3H_2O \tag{5.1}$$

$$SnO_2 + 4H^+ \rightarrow Sn^{4+} + 2H_2O \tag{5.2}$$

For Silver (Ag), the possible reaction with nitric acid is suggested below:

$$2Ag + 2HNO_3(aq) \leftrightarrow 2AgNO_3(aq) + H_2(g) \tag{5.3}$$

$$3Ag + 4HNO_3(aq) \leftrightarrow 3AgNO_3(aq) + NO(g) + 2H_2O \tag{5.4}$$

$$Ag + 2HNO_3(aq) \leftrightarrow AgNO3(aq) + NO_2(g) + H_2O \tag{5.5}$$

It is shown that inorganic acids(HNO_3,H_2SO_4) of high concentration could be used for digestion because of their behavior as a strong oxidizing agent. Nitric acid is used to dissolve metals whose E^o (standard reduction potential) values are greater than hydrogen. Selenides in CIGS are more susceptible to oxidation and structural damage. In practical terms, how the reaction might occur is influenced by several factors, and the behavior of the metals cannot be predicted from the potentials alone. Previous research on the separation and leaching effect on the spent CIGS solar in nitric acid systems reported that within 4 hours, leachate rates of 98.74% Cu, 95.55% In, 60.22% Ga and 3.18% Se could be achieved using 3.2 mol/L nitric acid concentration, the liquid-to-solid ratio of 9 mL/g, leaching temperature of $90°C$[42].

From the literature[35], the possible reaction between the CIGS layer and nitric acid was evaluated by studying the simple selenides (Cu_2Se, In_2Se_3 and Ga_2Se_3) present in the CIGS Layer. In the literature, it was reported that the Ag reactions with NO_x formation was found to be spontaneous for reactions 5.4 and 5.5. For Mo present in the metallic form, the formation of molybdic acid, $MoO_3 \bullet H_2O$, seems thermodynamically favored to be formed during the reaction.

Stainless steel consists of Fe and Cr and some impurities. For Corrosion resistance, nitric acid is used for the passivation of the stainless steel by creating a chromium oxide layer, with some Fe also being removed from the surface during this process. The passivation treatment in the industry is quick and does not take more than 1 h, while the temperature needed can even be as low as room temperature [43].

5.1.1 Whole solar cell

The whole solar cell was used to determine the total mass of each metal with 8M HNO_3. This experiment was carried out at room temperature for 28 hours. The surface area to liquid ratio of 1:3 cm^2/ml and stirring speed of 100rpm were used. All the experiments were done in triplicates, and the standard deviation in the plot was calculated based on them. The results are indicated in Figure5.1 below. It consists of two plots in which the high mass of metals(Ag, Mo, Se, In, Cu, Zn) and the low of them(Fe, Ga, W, Ti, Cr, Sn, Mg) are separated.

From Figure 5.1, it is observed that most of metals have a stable tendency during the leaching. While Fe and W show a considerable increment from 1 hour to 4 hours, Ti rises gradually and peaks 2.1mg/cell at 24 hours. The standard deviation showed a high value around 4 hours from both plots.

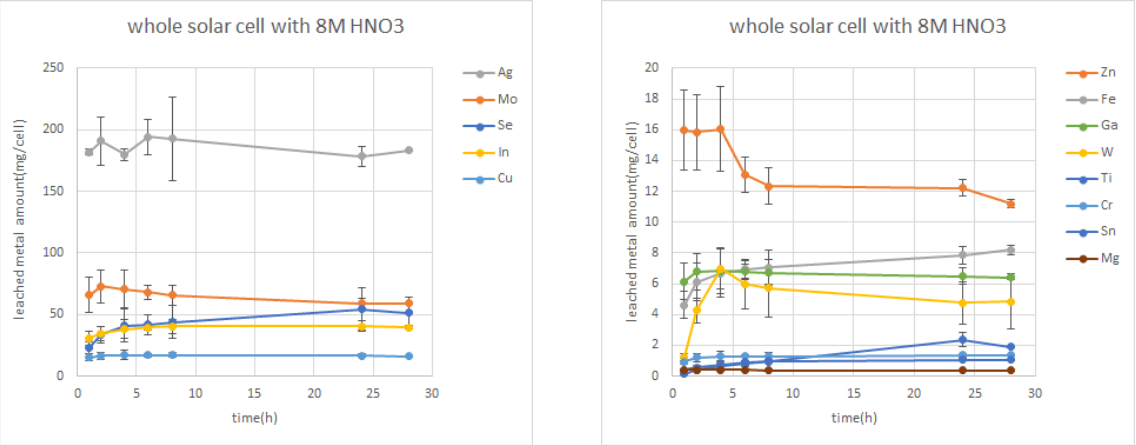

Figure 5.1: Mass of metals in whole solar cell complete digestion(conditions: 8M HNO3, room temperature, 100rpm, surface area to liquid ratio of 1:3).

In Table 5.1, the highest values of each metal was chosen from 1 hour to 28 hours of the digestion. The following data obtained from the 5.1 was set as a reference point to compare the results for the acids used in the following section.

Table 5.1: Mass of each metal element in 8M HNO_3.

element	concentration (ppm)
Ag	193.99 ± 33.95
Mo	72.70 ± 15.37
Se	54.49 ± 17.53
In	40.61 ± 7.82
Cu	17.20 ± 3.84
Zn	16.03 ± 2.75
Fe	8.19 ± 1.50
W	6.98 ± 1.86
Ga	6.83 ± 1.46
Ti	2.35 ± 0.19
Cr	1.35 ± 0.32
Sn	1.07 ± 0.14
Mg	0.41 ± 0.09

5.1.2 Big sample

In this experiment, the CIGS solar cell was equally divided into four pieces. One random piece of the solar cell was taken and leached with 8M HNO_3 at the same conditions as the previous sample. Figure 5.2 could be used to compare the results to confirm that the metals are evenly distributed on the solar cell. It was observed that the maximum Ag amount leached was 109.07mg/cell at 24 hours.

Figure 5.2 illustrates that several high-mass metals all reached the biggest mass at 24 hours and dropped after that. Considering the high standard deviation of these metals at 28 hours, this trend seemed to be not convincing. After 24 hours, the concentration of W decreased rapidly due to the precipitation of W to tungstic acid (H_2WO_4) in the presence of an acidic medium caused by exposure to oxygen during sample collection from the leaching container or due to atomic adsorption of oxygen on W [35, 44, 45].

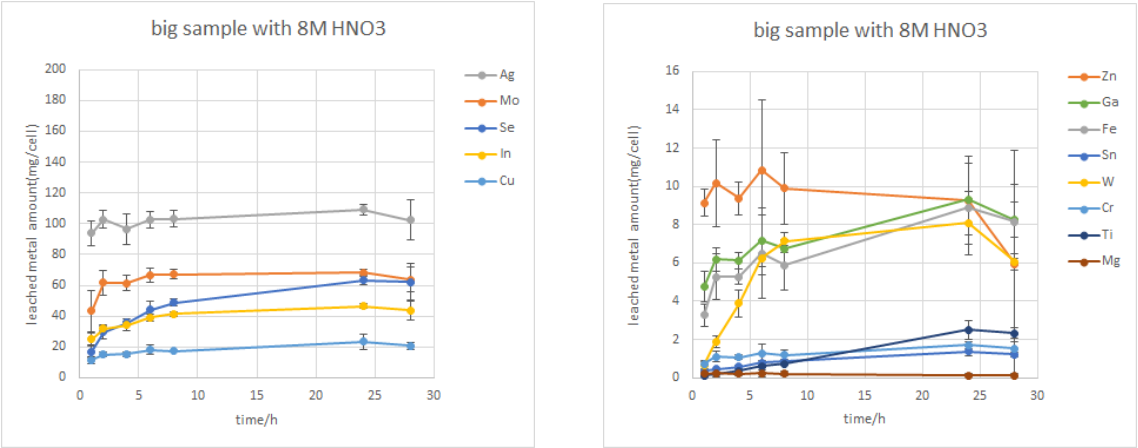

Figure 5.2: Mass of metals in big sample complete digestion(conditions: 8M HNO3, room temperature, 100rpm, surface area to liquid ratio of 1:3).

Table 5.2 indicates the largest mass of metals when the solar cell was divided into four equal big samples from 1 hour to 28 hours of digestion.

Table 5.2: Mass of each metal element in big sample with 8M HNO_3.

element	concentration (ppm)
Ag	109.07 ± 3.46
Mo	68.11 ± 2.16
Se	63.11 ± 3.06
In	46.53 ± 1.72
Cu	23.38 ± 4.74
Zn	10.86 ± 3.68
Fe	8.89 ± 0.84
W	8.09 ± 1.66
Ga	9.33 ± 1.88
Ti	2.49 ± 0.47
Cr	1.70 ± 0.16
Sn	1.36 ± 0.25
Mg	0.24 ± 0.17

5.1.3 Small sample

In this section, the $2.3 \times 5\ cm^2$ rectangle solar cell sample was chosen to carry out the leaching process. The experiment conditions were the same as in the previous two scenarios.

Figure 5.3 was observed that most of the metals had a complete dissolution at 4 hours due to the less leaching solution had better contact between oxygen and sample. But, the loss of the surface layer in cutting lead to a considerable reduction of Ag. 94.95mg/cell of Ag was the highest amount during the leaching process.

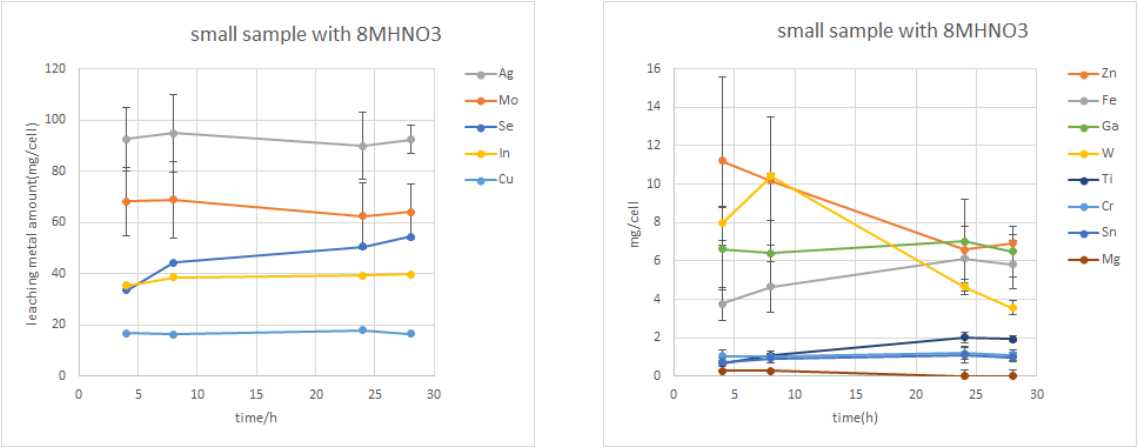

Figure 5.3: Mass of metals in small sample complete digestion(conditions: 8M HNO3, room temperature, 100rpm, surface area to liquid ratio of 1:3).

Table 5.3: Mass of each metal element in small sample with 8M HNO_3.

element	concentration (ppm)
Ag	94.95 ± 15.21
Mo	68.93 ± 14.88
Se	54.55 ± 9.62
In	39.70 ± 10.12
Cu	17.92 ± 5.79
Zn	11.20 ± 4.36
Fe	6.12 ± 1.70
W	10.42 ± 0.17
Ga	7.03 ± 2.15
Ti	2.06 ± 0.27
Cr	1.21 ± 0.35
Sn	1.11 ± 0.39
Mg	0.29 ± 0.11

After the comparison of the element composition among different sample preparations. The leaching amount of Ag in the whole solar cell was 193.99mg/cell which was higher than that in big and small sample(109.07 and 94.95mg/cell, respectively). One of the reason was the flakes loss from the surface where Ag was mainly present in the cutting process. On the other hand, the overlap of samples also influenced the contact between the leaching solution and samples. The different thickness of the layers and grain size also contributed to such large errors in total mass of metals.[35]

5.2 Organic acid leaching

Organic acids are organic compounds with acidic properties, classified based on the number of carboxylic functions. The mobilization and leaching of metals from solid samples such as solar cells by organic acids are based on the following two principles: acidolysis and complexolysis[46]. In acidolysis, the acid is dissociated to release protons to the medium around the surface of the cell sample. The metals are separated from the leachate solution. The released proton during acidolysis weakens the metal-ion bonds, causing the metal to go into solution. The organic acid dissociates the H^+ to promote the dissolution.process[47]

$$RCOOH + H_2O \rightleftharpoons RCOO^- + H_3O^+ \tag{5.6}$$

The reduction of protons generates hydrogen and oxidises the metal,

$$2H_3O^+ + 2e^- \rightarrow H_2 + 2H_2O \tag{5.7}$$

$$M \rightarrow M^{2+} + 2e^- \tag{5.8}$$

where M-metal; R= organic substituent group

.

In the complexation mechanism, the metals are extracted through ligand formations of the previously leached metal to form soluble complexes. The strength of the organic acids is generally based on several components, such as the acid dissociation constant (pKa) and the relative stability of the conjugate base of the acid. The acidolysis mechanism complements complexolysis through the stabilization of metal ions produced during acidolysis. The stability of metal complexes in the solutions minimizes the toxic effect of metal ion The organic acids possess strong complexing properties and have fewer environmental risks such as corrosion resistance of the equipment, absence of secondary pollution, and selective leaching behavior of the valuable metals. Moreover, the organic acid with a higher number of carboxyl groups that can form coordinate covalent bonds with metal ions led to higher leaching as the formed ligand is more stable.

5.2.1 Selection of citric acid

The potential for metal removal of citric acid relies on the total number of carboxylic groups present in the structure of this organic acid (three carboxylic groups).
This explanation has been proposed for its high efficiencies compared to other organic acids with fewer than three carboxylic groups. Above in Figure 5.4 are shown the reactions of the citric acids in leaching processes, including both acidolysis (liberation of protons and pKa values) and complexolysis (OA– metallic complex formation) mechanisms, previously reported, where Mn+ and M represent the metal ions [48].

Citric 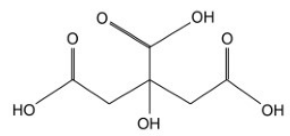	a) $C_6H_8O_7 \rightarrow C_6H_7O_7^- + H^+$ b) $C_6H_7O_7^- \rightarrow C_6H_6O_7^{2-} + H^+$ c) $C_6H_6O_7^{2-} \rightarrow C_6H_5O_7^{3-} + H^+$	3.09 4.75 6.40	a) $n[C_6H_7O_7^-] + M^{n+} \rightarrow M[C_6H_7O_7]_n$ b) $n[C_6H_6O_7^{2-}] + M^{n+} \rightarrow M_2[C_6H_6O_7]_n$ c) $n[C_6H_5O_7^{3-}] + M^{n+} \rightarrow M_3[C_6H_5O_7]_n$

Figure 5.4: Reactions involved in acidolysis and complexolysis mechanisms for metal recovery[4].

5.2.1.1 Effects of concentration

The solar cell samples in this section were divided into $2.3 \times 5\ cm^2$ rectangles. These samples were leached with 1M, 0.5M, 0.1M, and 0.01M citric acid at room temperature. The surface area to liquid ratio of 1:3 and stirring speed of 100rpm was set for the experiments. The Figure 5.5 indicates the mass of five metals (Zn, In, Mo, and Sn) during the leaching process and helps determine the optimal concentration of citric acid.

Figure 5.5a indicates the mass of five valuable metals in 1M citric acid. It is found that all the metals have an increment from 1 hour to 2 hours and then slightly fluctuate. Except for Mo, the curve gradually goes up and peaks at 2.6mg/cell at 28 hours. Meanwhile, a significant drop of Ag and In after 24 hours is observed.

Figure 5.5b shows a similar tendency as 1M citric acid, except Zn and In have an opposite tendency after 24 hours, they rise up to 11.74mg/cell and 7.38mg/cell, respectively.

Figure 5.5c illustrates that relatively the highest mass in Zn, Mo and Fe compared to 1M and 0.5M citric acid cases. Meanwhile, the curve of Mo keeps increasing until 28 hours, and other metals are observed to reach their peak around 8 hours.

Figure 5.5d presents that the Zn and In curves have unstable ups and downs fluctuations during the leaching process, the mass per cell could be reached to 11.60 and 5.99 at 28 hours. The mass of the rest metals is likewise slightly lower than the other concentration scenarios.

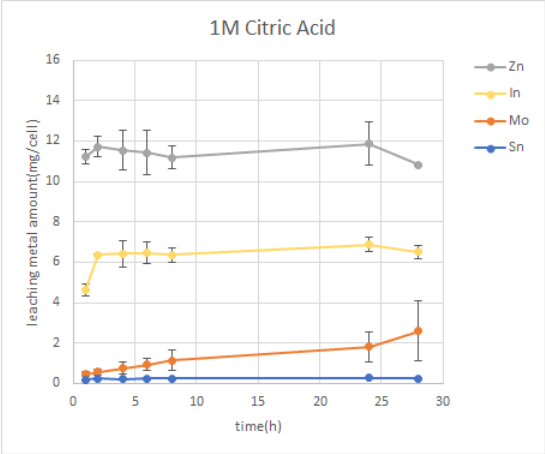

(a) 1M citric acid

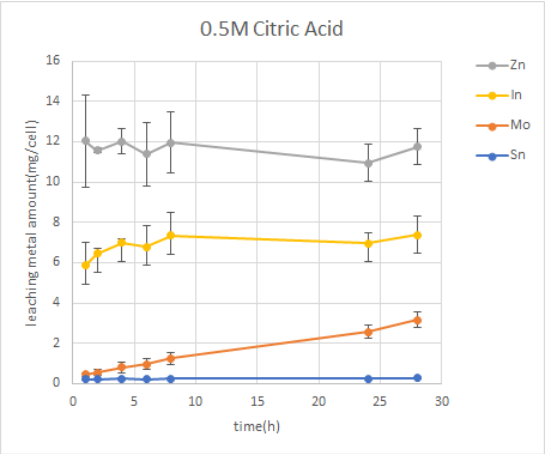

(b) 0.5M citric acid

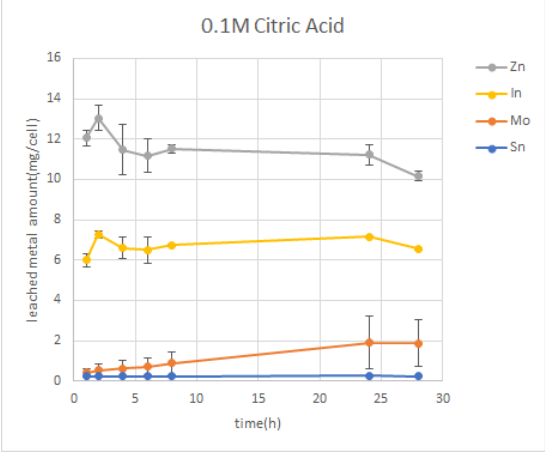

(c) 0.1M citric acid

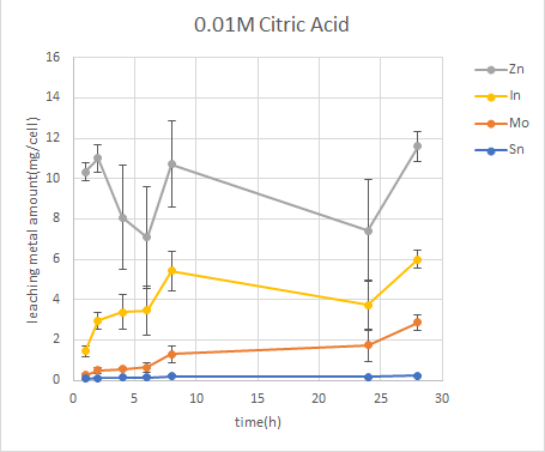

(d) 0.01M citric acid

Figure 5.5: Plots of mass of each element at 1M, 0.5M, 0.1M, 0.01M citric acid(conditions: room temperature, stirring speed of 100rpm, surface area to liquid ratio of 1:3).

After carrying out the experiments at 1M, 0.5M, 0.1M, and 0.01M citric acid, the highest leaching amount of Zn, Sn, In, Mo, and optimal time were chosen in Table 5.4. The experiment conditions could be as the reference to achieve an effective leaching.

Table 5.4: The highest concentration and mass of metal at 1M, 0.5M, 0.1M, and 0.01M.

Metal	Concentration (ppm)	Mass (mg/cell)	Time (h)	Condition
Zn	1.88	13.05 ± 0.63	2	0.1M
Sn	0.04	0.26 ± 0.01	24	1M
In	0.03	7.38 ± 0.92	28	0.5M
Mo	0.30	1.90 ± 1.30	24	0.1M

5.2.1.2 Effects of the surface area to liquid ratio

Teknetzi et al.[35] leached the CIGS solar cell with 0.5M and 2M HNO_3, and it was found that the increased surface area to liquid ratio contributed to the increased yield for most metals. Not only the accumulation of counter ions may promote the metal leaching, but also the mixture of the solar cell and oxygen which was the oxidizing agent. So, 1M citric acid was chosen as the highest acid strength tested before to carry out the experiment at different surface area to liquid ratios.

From Figure 5.6b, all these metals had a gradual increment from 1 hour to 8 hours. Among them, In had the largest growth rate which the mass per cell increasing from 5.10 to 7.14mg/cell. Nevertheless, only Mo maintained an upward trend, other metals increased in the beginning 8 hours and then had a certain amount of ups and downs.

Figure 5.6c showed that the mass of Zn and In kept rising from 1 hour to 8 hours and the highest value were 16.8 and 11.0mg/cell, respectively. The Mo curve gradually increased and peaked at 1.86mg/cell at 28 hours.

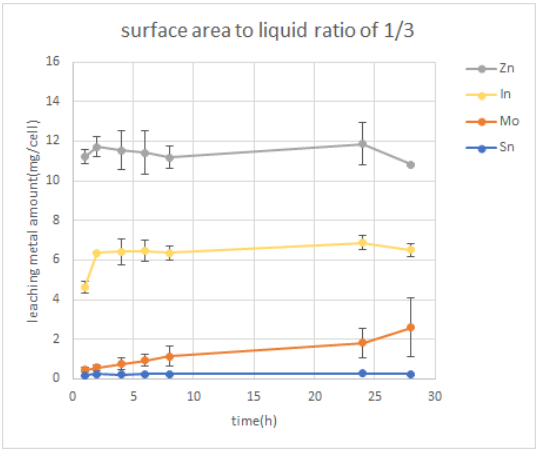

(a) Surface area to liquid ratio of 1:3

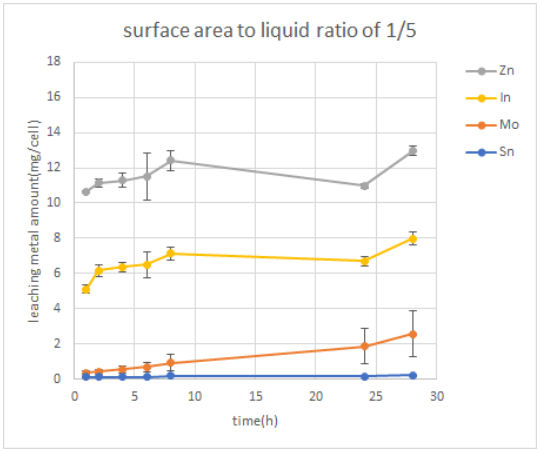

(b) Surface area to liquid ratio of 1:5

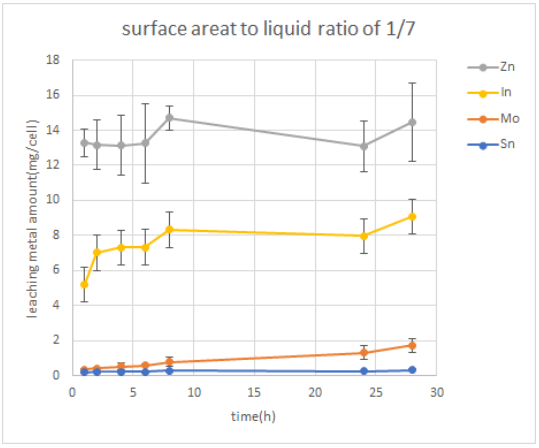

(c) Surface area to liquid ratio of 1:7

Figure 5.6: Plots of mass of five metal at a surface area to liquid ratio of 1:5 and 1:7(conditions: 1M citric acid, room temperature, stirring speed of 100rpm).

Table 5.5 represents the maximum concentrations of Zn, Sn, In, Mo obtained via 1M citric acid leaching at the different surface area to liquid ratio of 1:3, 1:5 and 1:7.

Table 5.5: The highest concentration and mass of metal at surface area to liquid ratio of 1:3, 1:5, and 1:7.

Metal	Concentration (ppm)	Mass (mg/cell)	Time (h)	Condition
Zn	0.92	14.72 ± 0.69	8	1:7
Sn	0.02	0.31 ± 0.07	28	1:7
In	0.57	9.08 ± 1.71	28	1:7
Mo	0.40	2.60 ± 1.46	28	1:3

5.2.1.3 Effects of temperature

In order to analyze the impact of additional variables, it was determined that using 1M citric acid rather than 0.1M citric acid would be more suitable as it is less likely to vaporize easily. Hu et al.[19] investigated the effect of temperature on CIGS material with 3.2M HNO_3. It could be seen that the leaching amount of Se and In reached the peak at 70°C while Ga and Cu increased until 90°C. As a result, room temperature, 50°C and 80°C were chosen to operate the leaching process. Considering the effect of evaporation on this experiment, it was carried out by a quarter of the solar cell with 1M citric acid with a surface area to liquid ratio of 1:3 for 8 hours.

According to Figure 5.7a, the leaching amount of Zn, In, and Sn reached a peak at 2 hours, and the curve of In showed a bigger decrease than Zn after that until 28 hours. Mo kept a stable rise in the first 24 hours and converged.

Based on Figure 5.7b, the curve of Zn reached the highest leaching amount at 4 hours and In kept increasing until 8 hours. The maximum leaching amount of Zn and In were 13.39 and 13.41mg/cell, respectively. W was shown as a new metal with a similar curve but slightly lower than Mo. At the same time, the leachate was observed to black and purple. This experiment stopped at 8 hours since the loss of citric acid.

From Figure 5.7c, it was apparent that the curve of In rises rapidly over time and the biggest mass of 21.69mg/cell was reached at 8 hours. Except for Zn, which had the highest mass in the beginning and then fluctuated slightly, the rest of the metals rise slowly. Since the direct contact of the hot plate and glass substrate, Fe and Cr had an especially high concentration as well.

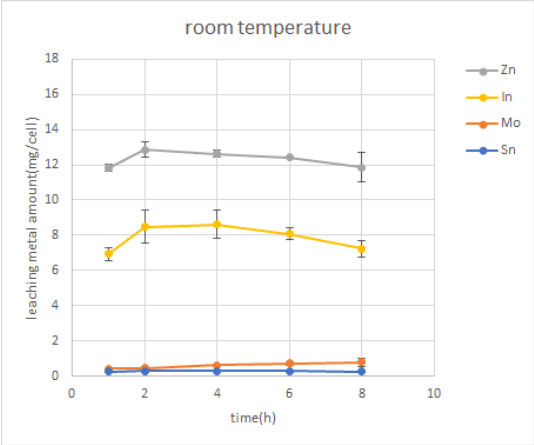

(a) room temperature

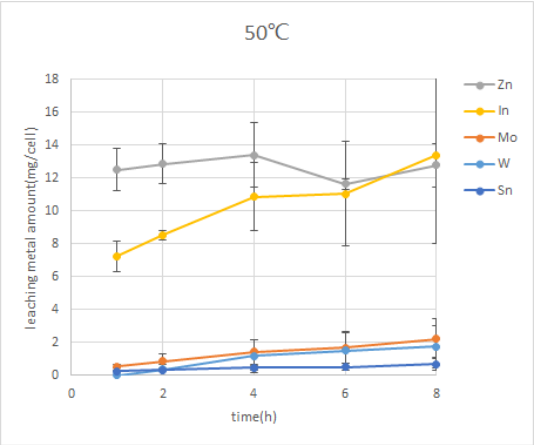

(b) $50°C$

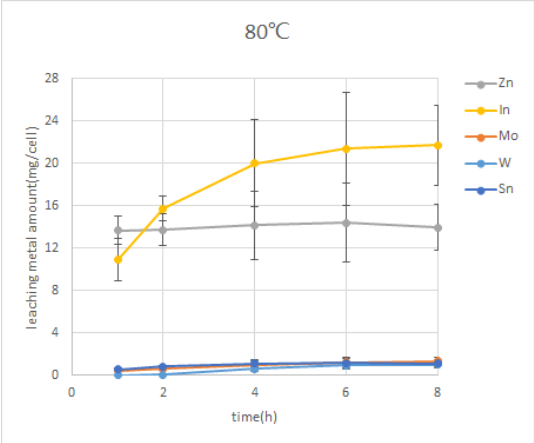

(c) $80°C$

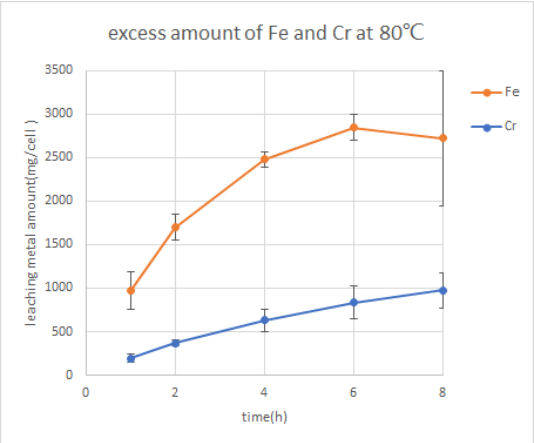

(d) $80°C$

Note: the amount of Fe and Cr was out of the calibration range

Figure 5.7: Plots of mass of metals at room temperature, $50°C$ and $80°C$(conditions: 1M citric acid, surface area to liquid ratio of 1:3, stirring speed of 100rpm).

Table 5.6 presents a summary of the maximum concentrations of various metals obtained via 1M citric acid leaching at different temperatures, namely room temperature, 50°C, and 80°C.

Table 5.6: The highest concentration and mass of metal at room temperature, $50°C$, $80°C$.

Metal	Concentration (ppm)	Mass (mg/cell)	Time (h)	Condition
Zn	1.83	12.86 ± 0.43	2	room temperature
In	5.59	21.69 ± 3.80	8	$80°C$
Mo	0.32	2.23 ± 1.20	8	$50°C$
Sn	0.22	1.16 ± 0.41	6	$80°C$
W	0.25	1.77 ± 1.29	8	$50°C$

To gain a deeper understanding of the elevated levels of Fe and Cr, as well as to identify any impurities in the precipitate, SEM-EDS analysis was conducted on the sample extracted from the leaching solution at a temperature of 80°C. The investigation results are presented visually in Figure 5.8.

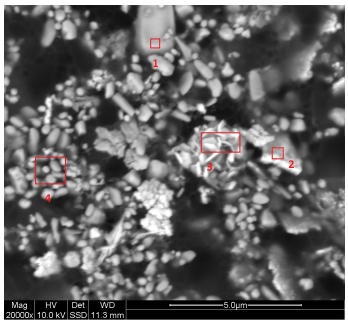

(a) Spot 1, 2, 3, and 4

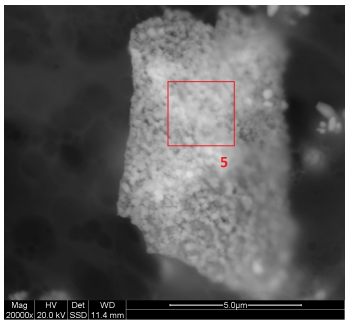

(b) Spot 5

Figure 5.8: SEM image of the precipitate from the leaching solution when the leaching temperature was 80°C.

Here, the SEM analysis was done using the backscattered electron imaging of the precipitate. Additionally, an EDS analysis was performed to obtain a clearer understanding of the elemental composition for each of the spots(1-5) that have been marked in figure 5.8a and figure 5.8b. Spot 5 is a magnified view of the same area as spot 1, but a higher voltage setting was applied to make the image capture more precise and detailed, allowing for a more comprehensive examination of spot 1. The energy spectrum of the analyzed spots is exhibited in Figure 5.9 and Figure 5.10.

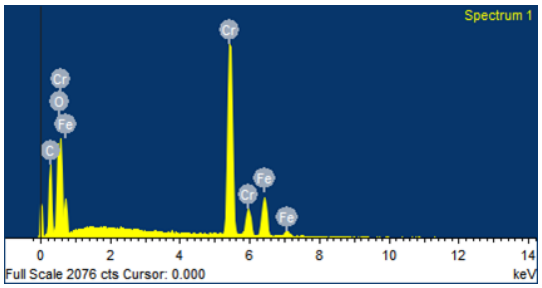

(a) Spectrum 1

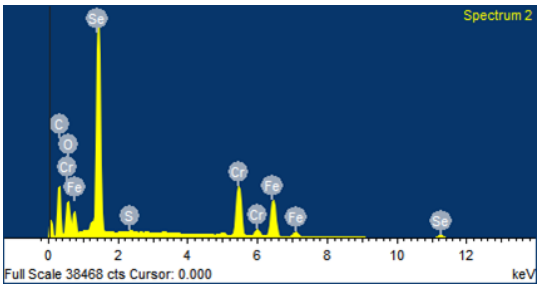

(b) Spectrum 2

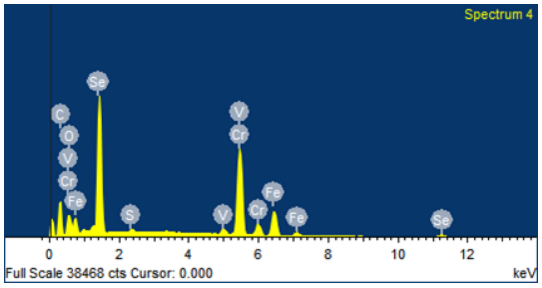

(c) Spectrum 3

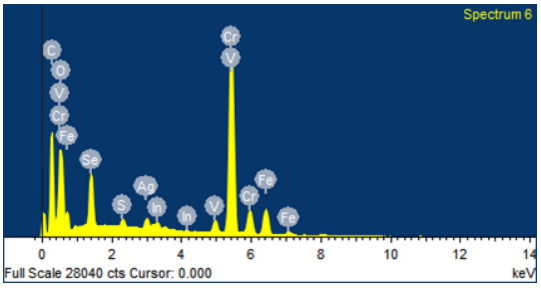

(d) Spectrum 4

Figure 5.9: EDS images of spectrum 1, 2, 3, and 4

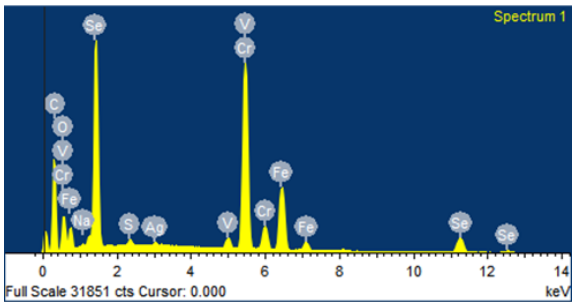

Figure 5.10: EDS images of spectrum 5.

The table 5.7 provides information on the weight percentage of the elements identified in the EDS spectrum for each spot.The biggest cluster of particles in the precipitate (spot 1) exhibited high Cr, Fe, oxygen, and carbon concentrations in the spectrum plot 5.9a. The carbon might be due to the presence of a polycarbonate substrate or due to an organometallic compound formed in the leaching solution and the chromium; Fe might be due to the reduction of Cr^{6+} to Cr^{3+} in the presence of Fe^{3+} as a catalyst. One reason for the following outcome can be explained by understanding the effect of citrate on the hexavalent chromium in the presence of Fe source material. In the environment, chromium is present in two valence states: trivalent chromium and hexavalent chromium. In terms of their toxicity and solubility, Cr^{3+} and Cr^{6+} exhibit notable differences. Specifically, Cr^{3+} is characterized by its water-insolubility and relatively lower toxicity, while Cr^{6+} is water-soluble and more toxic. In previous studies[49, 50], it has been found that aqueous Fe^{2+} has the ability to reduce Cr^{6+} to Cr^{3+}. In other studies[51], it was observed that soluble Fe^{3+} could promote the Cr^{6+} reduction by organic ligands. Fe^{3+} can form complexes with organic ligands and then these complexes could be reduced to Fe^{2+}-ligand complexes through photo-reduction. In our experiment, the high-temperature condition ($80°C$) caused the catalytic effect of soluble Fe^{3+} on Cr^{6+} reduction. This might be the reason for the enhanced amount of Cr present in the precipitate[52, 53, 54]. For the flake particles(spot 2 and spot 3), the EDX results 5.9b and 5.9c showed large amounts of Se present in the precipitate, which might occur due to the unreacted samples present in the form of metal selenides. Moreover, for the minute flakes (spot 4), the EDX 5.9d accounted for a small amount of Ag and In, which was not observed in any other precipitate particles. The Ag might occur due to the agitation caused by the high temperature of the leaching solution or maybe due to the wear and tear of the Ag layer at the time of collecting the sample after the leaching is over. In contrast, In might be due to the formation of indium citrate complexes or due to agitation.

Table 5.7: EDS analysis of the different spots (in weight %).

Spot	C	O	S	Cr	Fe	Se	V	Ag	Na	In
1	18.80	2.58	-	59.24	19.38	-	-	-	-	-
2	27.56	6.32	0.25	16.63	19.00	30.24	-	-	-	-
3	21.11	3.82	0.38	33.34	15.47	24.05	1.82	-	-	-
4	24.81	6.7	0.53	45.50	10.27	5.98	2.47	2.26	-	1.48
5	36.83	7.38	0.26	23.13	11.86	18.75	1.21	0.44	0.13	-

The XRD technique (figure 5.11) was applied to the precipitate to acquire the data about the crystallographic structure. The XRD analysis resulted in an amorphous spectrum with broad peaks.

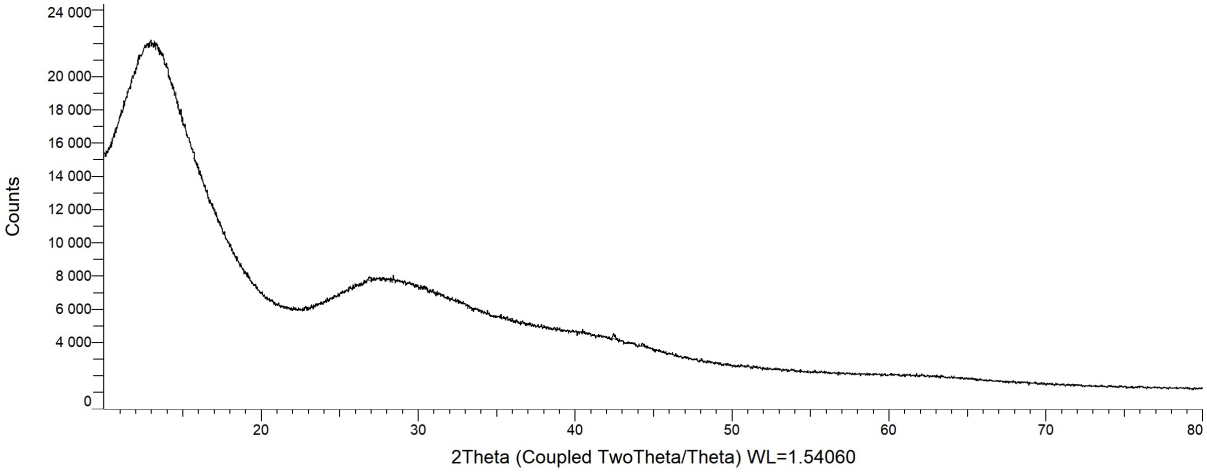

Figure 5.11: XRD results of the precipitate.

5.2.1.4 Effects of stirring speed

Generally, if the agitation is intensified, the leaching rate increases until a saturation level is attained, after which it may decrease. The main aim is to cause shrinkage of the liquid film and increase the available surface area of the samples, making the diffusion and reaction much easier[55]. On the other hand, harsh agitation can delay the diffusion of ions onto the surface of the unreacted sample caused by flow problems(such as vortex formation, bubbling, etc.)[56, 57]. The mode of contact between solids and liquids plays a huge essential role in the kinetics of leaching.

From Figure 5.12, it was apparent that the leaching amount of Zn and In were both high at the beginning 2 hours, and they had a pretty similar trend during the leaching process. The mass of In reached the peak of 7.62mg/cell at 24 hours. There was a constantly increased leaching amount of Mo, and a bit amount of Sn was observed. No substantial increment of these four metals was seen when the stirring speed rose from 100 rpm to 200 rpm because the majority of the leaching solution flowed around the wall under centrifugal force[58], then it might have a negative impact on the contact between the leaching solution and the surface of the solar cell.

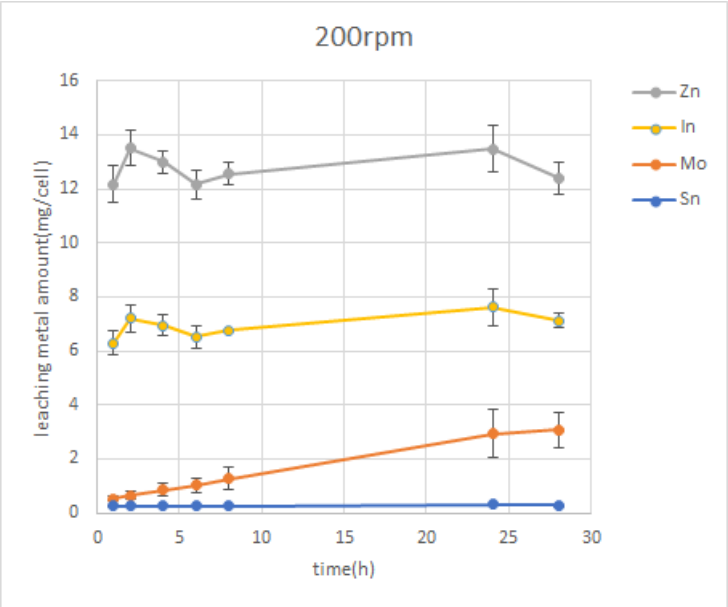

Figure 5.12: Plots of mass of metals at 200rpm(conditions: 1M citric acid, surface area to liquid ratio of 1:3, room temperature).

5.2.2 Selection of tartaric acid

Marafi et al.[59] investigated the recovery of metal from spent catalyst by organic acid leaching and found that tartaric acid had a highly selective extraction of Mo since almost 93% of Mo could be dissolved in 5wt% tartaric acid at $50°C$ by ultrasonic agitation in an ultrasonic bath. Due to the good leaching yield of Mo, tartaric acid might be an opportunity to be the first step leaching for the removal of Mo and some potential metals and thus the leaching of CIGS cells in tartaric acid was investigated.

5.2.2.1 Effect of concentration

Jonas et al.[60] used 1M DL-tartaric acid and organic acid to investigate the recovery of In and Mo from ITO glass samples of LCD screens. The leaching amount of Mo by DL-tartaric acid was higher than that by organic acid leaching. In order to find out the effect of concentration on metals and control the cost, 1M and 0.5M DL-tartaric acid was used to carry out the experiment.

According to the results from Figure 5.13a, the most amount of Zn and In were leached from 6 hours of the leaching and the mass of then were 12.33 and 7.68mg/-cell, respectively. Mo dissolution occurred from 1 hour and W dissolution was from 3 hours. Both of these metals were observed to increase linearly with time. The mass per cell of 9.67 and 8.22 were obtained at 28 hours.

Figure 5.13b indicated that the curve of Zn and In fluctuated at almost same trend. At the same time, the amount of them were slightly higher than that with 1M citric acid. Besides, all of these metals had a stable or increased tendency from 8

hours to 24 hours. For Mo and W, the growth rate had become significantly slower after 24 hours and the amount still reached about 9.12 and 7.50mg/cell at 28 hours, respectively.

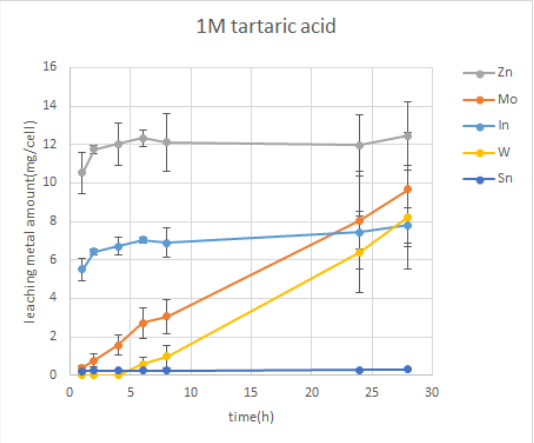

(a) 1M tartaric acid

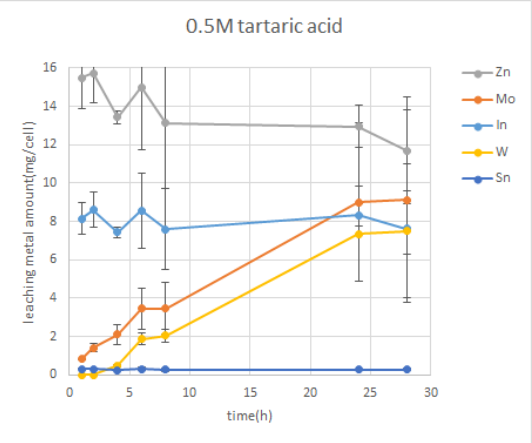

(b) 0.5M tartaric acid

Figure 5.13: Plots of mass of metals at 1M and 0.5M tartaric acid(conditions: room temperature, surface area to liquid ratio of 1:3, stirring speed of 100rpm).

5.3 Discussion

To sum up, this thesis mainly investigated the leaching yield of the valuable metals in CIGS solar cells with inorganic acid by different division methods, and organic acids at different concentrations, surface area to liquid ratio, and temperature.

On the one hand, the effect of different division methods was studied to determine the distribution of the CIGS solar cell. Considering the leachable metals except steel substrate in the nitric acid, the results showed that only the mass of Ag in the whole solar cell was 44% higher than that in big samples and small samples. It was mainly because of the loss of the grid contact layer when cutting. As a result, it is beneficial to leach the valuable metals with the whole solar cell on the industrial scale to avoid this circumstance. For the majority of the metals, such as Ag, Zn was found to have almost complete leaching in the beginning 2 hours. Due to the fact that these metals were located in the grid contact layer and window, buffer layers, which were exposed to leaching solution. Mo increased linearly over time, it mainly existed in the Mo back contact layer which was not the first layer to contact with the leaching solution, which means that leachate etches effectively from the edges and can penetrate between the layers.

Moreover, the concentration of citric acid and tartaric acid, surface area to liquid ratio, temperature and agitation were considered to compare the results. It can be seen that leaching amount of Zn, In, Mo, Sn had a slight change when the concentration of citric acid and surface area to liquid ratio increased. Especially the

leaching amounts of Zn and In were almost 90% and 25% compared to 8M HNO3, respectively. Mo only had a slight increment when changing these two parameters. In addition, the leaching amount of Zn and In always dropped after 4 hours until 24 hours. When the sealed plastic container was opened and the sampling was completed, the leaching rate increased again. The main factor was regarded as the soluble oxygen, which will affect the leaching process. So, carrying out the leaching process by the solar cell with 1M citric acid at room temperature, surface area to liquid ratio of 1:3, stirring speed of 100rpm could be an option to remove Zn and some quantity of In.

Temperature is a significant parameter to affect the leaching process due to the fact that it showed Fe from the glass substrate at the bottom layer had a pretty high leaching yield. At the same time, a considerable amount of Cr was leached as well when the temperature changed from room temperature to $80°C$. The higher amount of Cr presents can be attributed to the existence of citrate, which promotes the catalytic influence of Fe^{3+} soluble complexes about the reduction of Cr^{6+} to Cr^{3+}. The leaching yield of In was 53.41% at $80°C$, which was higher than other researcher's results that the leaching yield of In increased before $70°C$[19]. Since the material in that research was only spent CIGS, it was further verified that In was also present in large quantities on top layers of CIGS solar cell. Besides, both room temperature and $50°C$ can be used to achieve the full leaching of Zn. Complete leaching of Zn and Sn was obtained when the temperature was $80°C$. Simultaneously, under this condition, a good leaching of In was observed and the amount was almost 60% compared to the sample with 8M HNO_3. Given the substantial levels of Fe and Cr leaching observed in the precipitate at $80°C$, it would be effective to consider leaching solar cells with a glass substrate as opposed to those with a steel substrate.

Tartaric acid has a pretty similar leaching amount of Zn and In, so it might be an alternative organic acid when it comes to Zn and In. In addition, during the whole leaching process, Mo and W dissolution are observed to take place. Leaching the CIGS solar cell with tartaric acid at mild conditions may be feasible for the recovery of Zn, In, Mo, and W.

6
Conclusion

In the thesis, three different division methods were applied to cut the CIGS solar cell to investigate the effect of sample size and preparation for the leaching process of the metals. For 8M HNO_3, except Ag, the concentration of other leached metals was very similar in these three scenarios. So, these metals can be assumed to be equally distributed on the solar cell, the differences in grain size when manufacturing does not have a huge impact on leaching yield. As for Ag, the cutting loss might be the main factor in affecting the mass from 193mg/cell to 109mg/cell.

When the experiments were carried out at the surface area to liquid ratio of 1:3, stirring speed of 100rpm and room temperature, the concentration of citric acid all indicated more than 80% of Zn was leached compared to 8M HNO_3. In addition, almost complete leaching of Zn is achieved when the surface area to liquid ratio of 1:7, stirring speed of 100rpm, room temperature, and 1M citric acid are used. It would be a good option to remove Zn under these conditions. Furthermore, ICP-OES measurements reveal significant concentrations of Fe and Cr when the temperature is $80°C$. The precipitate found in the leaching solution was studied using SEM-EDS analysis, it is mainly attributed to the reduction of Cr^{6+} to Cr^{3+} in the presence of the aqueous Fe^{2+} or might be due the formation of chromium-citrate complexes. Regarding tartaric acid, the leaching of W was observed and its leaching yield of 92% was reached at 24 hours. As a result, organic acids like citric acid and tartaric acid can be used to leach Zn and W at specific conditions as mentioned above, respectively.

6.1 Further Research

As the results above, the airflow could be taken into account during the leaching process, especially when the citric acid is used. Except for the introduction of oxidizing agents like oxygen, H_2O_2 is another alternative chemical to add to the organic acids. It can be done to understand whether the presence of the metal ions present in the CIGS solar cells creates a synergistic effect on the leaching.

When it comes to the recovery of Mo and W with tartaric acid leaching, the leaching time would be a factor to influences the leaching yield of them. Since the longer leaching time and constant increased curve, an appropriate extension of reaction time leads to complete leaching.

In order to progress for further research, one thing that can be considered is to selectively leach the Zn contained layer using low-concentrated acids in a short leaching duration in a single step and then check whether the prior step could improve the selective leaching behavior of the metals of the CIGS sample using organic acid.

Bibliography

[1] Iea-pvps Irena. End-of-life management: Solar photovoltaic panels. *International Renewable Energy Agency and International Energy Agency Photovoltaic Power Systems*, 2016.

[2] Elaheh Ghorbani, Janos Kiss, Hossein Mirhosseini, Guido Roma, Markus Schmidt, Johannes Windeln, Thomas D Kuhne, and Claudia Felser. Hybrid-functional calculations on the incorporation of na and k impurities into the cuinse2 and cuin5se8 solar-cell materials. *The Journal of Physical Chemistry C*, 119(45):25197–25203, 2015.

[3] Chiranjib Kumar Gupta. *Chemical metallurgy: principles and practice*. John Wiley & Sons, 2006.

[4] Itzel A Cruz-Rodríguez, Norma G Rojas-Avelizapa, and Andrea M Rivas-Castillo. Microbially-produced organic acids as leaching agents for metal recovery processes. *Postępy Mikrobiologii-Advancements of Microbiology*, 61(4):179–190, 2022.

[5] Nicole C McDonald and Joshua M Pearce. Producer responsibility and recycling solar photovoltaic modules. *Energy Policy*, 38(11):7041–7047, 2010.

[6] Annarita Paiano. Photovoltaic waste assessment in italy. *Renewable and Sustainable Energy Reviews*, 41:99–112, 2015.

[7] Piotr Bojek. Solar pv. 2021.

[8] Md Shahariar Chowdhury, Kazi Sajedur Rahman, Tanjia Chowdhury, Narissara Nuthammachot, Kuaanan Techato, Md Akhtaruzzaman, Sieh Kiong Tiong, Kamaruzzaman Sopian, and Nowshad Amin. An overview of solar photovoltaic panels' end-of-life material recycling. *Energy Strategy Reviews*, 27:100431, 2020.

[9] EC Directive. Directive 2012/19/eu of the european parliament and of the council of 4 july 2012 on waste electrical and electronic equipment, weee. *Official Journal of the European Union L*, 197:38–71, 2012.

[10] Michael Taylor, Pablo Ralon, and Andrei Ilas. The power to change: solar and wind cost reduction potential to 2025. *International renewable energy agency (IRENA)*, 2016.

[11] Fan-Wei Liu, Tzu-Min Cheng, Yen-Jung Chen, Kai-Chieh Yueh, Shin-Yi Tang, Kuangye Wang, Chia-Lung Wu, Hsu-Sheng Tsai, Yi-Jen Yu, Chih-Huang Lai, Wei-Sheng Chen, and Yu-Lun Chueh. High-yield recycling and recovery of copper, indium, and gallium from waste copper indium gallium selenide thin-film solar panels. *Solar Energy Materials and Solar Cells*, 241:111691, 2022.

[12] Jeyakumar Ramanujam and Udai P. Singh. Copper indium gallium selenide based solar cells – a review. *Energy Environ. Sci.*, 10:1306–1319, 2017.

[13] Yingwei Lv, Peng Xing, Baozhong Ma, Bao Liu, Chengyan Wang, Yonglu Zhang, and WenJuan Zhang. Separation and recovery of valuable elements from spent cigs materials. *ACS Sustainable Chemistry & Engineering*, 7(24):19816–19823, 2019.

[14] SeJin Ahn, ChaeWoong Kim, Jae Ho Yun, Jihye Gwak, Sunho Jeong, Beyong-Hwan Ryu, and KyungHoon Yoon. Cuinse2 (cis) thin film solar cells by direct coating and selenization of solution precursors. *The Journal of Physical Chemistry C*, 114(17):8108–8113, 2010.

[15] M. Kaelin, D. Rudmann, and A.N. Tiwari. Low cost processing of cigs thin film solar cells. *Solar Energy*, 77(6):749–756, 2004. Thin Film PV.

[16] Jong Won Park, Young Woo Choi, Eunjoo Lee, Oh Shim Joo, Sungho Yoon, and Byoung Koun Min. Synthesis of cigs absorber layers via a paste coating. *Journal of Crystal Growth*, 311(9):2621–2625, 2009.

[17] Vasilis Fthenakis. Sustainability of photovoltaics: The case for thin-film solar cells. *Renewable and Sustainable Energy Reviews*, 13(9):2746–2750, 2009.

[18] Baozhong Ma, Xiang Li, Bao Liu, Peng Xing, WenJuan Zhang, Chengyan Wang, and Yongqiang Chen. Effective separation and recovery of valuable components from cigs chamber waste via controlled phase transformation and selective leaching. *ACS Sustainable Chemistry & Engineering*, 8(7):3026–3037, 2020.

[19] Die Hu, Baozhong Ma, Xiang Li, Yingwei Lv, Yongqiang Chen, and Chengyan Wang. Innovative and sustainable separation and recovery of valuable metals in spent cigs materials. *Journal of Cleaner Production*, 350:131426, 2022.

[20] Nandang Mufti, Tahta Amrillah, Ahmad Taufiq, Sunaryono, Aripriharta, Markus Diantoro, Zulhadjri, and Hadi Nur. Review of cigs-based solar cells manufacturing by structural engineering. *Solar Energy*, 207:1146–1157, 2020.

[21] Kam Hoe Ong, Ramasamy Agileswari, Biancamaria Maniscalco, Panagiota Arnou, Chakrabarty Chandan Kumar, Jake W Bowers, Marayati Bte Marsadek, et al. Review on substrate and molybdenum back contact in cigs thin film solar cell. *International Journal of Photoenergy*, 2018, 2018.

[22] Anna MK Gustafsson, Mark R StJ Foreman, and Christian Ekberg. Recycling of high purity selenium from cigs solar cell waste materials. *Waste management*, 34(10):1775–1782, 2014.

[23] Zhi-yuan Ma, Hong-ying Yang, Song-tao Huang, Yang Lü, and Liu Xiong. Ultra fast microwave-assisted leaching for the recovery of copper and tellurium from copper anode slime. *International Journal of Minerals, Metallurgy, and Materials*, 22:582–588, 2015.

[24] Sébastien Jutteau. *Design, prototyping and characterization of micro-concentrated photovoltaic systems based on Cu(In,Ga) Se2 solar cells*. Theses, Université Pierre et Marie Curie - Paris VI, November 2016.

[25] CEM Meskers, K Vandenbroeck, J Vliegen, I De Ruijter, T Dalle, and P Rigby. Recycling technologies to close the loop for pv materials. In *25th European Photovoltaic Solar Energy Conference and Exhibition, 5th World Conference on Photovoltaic Energy Conversion, Valencia, Spain, 6th*, pages 3683–3687, 2010.

[26] Kari Larsen. End-of-life pv: then what? *Renewable energy focus*, 10(4):48–53, 2009.

[27] Lisa Krueger. Overview of first solar's module collection and recycling program. In *EPIA 1st international conference on PV module recycling*, volume 26, 2010.

[28] Marina Monteiro Lunardi, Juan Pablo Alvarez-Gaitan, José I Bilbao, and Richard Corkish. A review of recycling processes for photovoltaic modules. *Solar Panels and Photovoltaic Materials*, pages 9–27, 2018.

[29] Keiichi Komoto, Jin-Seok Lee, Jia Zhang, Dwarakanath Ravikumar, Parikhit Sinha, Andreas Wade, and Garvin A Heath. End-of-life management of photovoltaic panels: Trends in pv module recycling technologies. Technical report, National Renewable Energy Lab.(NREL), Golden, CO (United States), 2018.

[30] Jorge E De-la Cruz-Moreno, Agueda E Ceniceros-Gomez, Ofelia Morton-Bermea, and Elizabeth Hernandez-Alvarez. Recovery of indium from jarosite residues of zinc refinery by a hydrometallurgical process. *Hydrometallurgy*, 203:105697, 2021.

[31] Fan-Wei Liu, Gill Biesold, Meng Zhang, Rachel Lawless, Juan-Pablo Correa-Baena, Yu-Lun Chueh, and Zhiqun Lin. Recycling and recovery of perovskite solar cells. *Materials Today*, 43:185–197, 2021.

[32] Minas Theocharis, Petros E. Tsakiridis, Pavlina Kousi, Artin Hatzikioseyian, Ioannis Zarkadas, Emmanouella Remoundaki, and Gerasimos Lyberatos. Hydrometallurgical treatment for the extraction and separation of indium and gallium from end-of-life cigs photovoltaic panels. *Materials Proceedings*, 5(1), 2021.

[33] Max Marwede, Wolfgang Berger, Martin Schlummer, Andreas Mäurer, and Armin Reller. Recycling paths for thin-film chalcogenide photovoltaic waste–current feasible processes. *Renewable Energy*, 55:220–229, 2013.

[34] Alessia Amato and Francesca Beolchini. End-of-life cigs photovoltaic panel: A source of secondary indium and gallium. *Progress in Photovoltaics: Research and Applications*, 27(3):229–236, 2019.

[35] Ioanna Teknetzi, Stellan Holgersson, and Burçak Ebin. Valuable metal recycling from thin film cigs solar cells by leaching under mild conditions. *Solar Energy Materials and Solar Cells*, 252:112178, 2023.

[36] Manivannan Sethurajan, Piet NL Lens, Heinrich A Horn, Luiz HA Figueiredo, and Eric D van Hullebusch. Leaching and recovery of metals. *Sustainable Heavy Metal Remediation: Volume 2: Case studies*, pages 161–206, 2017.

[37] Arti J Majumdar and Nidhi Dubey. Applications of inductively coupled plasma-atomic emission spectrometry (icp-oes) in impurity profiling of pharmaceuticals. *International Journal of Pharmacy & Life Sciences*, 8(1), 2017.

[38] Sharib Raza Khan, Babita Sharma, Pooja A Chawla, and Rohit Bhatia. Inductively coupled plasma optical emission spectrometry (icp-oes): a powerful analytical technique for elemental analysis. *Food Analytical Methods*, pages 1–23, 2022.

[39] LRB Elton and Daphne F Jackson. X-ray diffraction and the bragg law. *American Journal of Physics*, 34(11):1036–1038, 1966.

[40] Daniel C Harris. *Quantitative chemical analysis*. Macmillan, 2010.

[41] Kaihua Zhang, Yufeng Wu, Wei Wang, Bin Li, Yinan Zhang, and Tieyong Zuo. Recycling indium from waste lcds: A review. *Resources, Conservation and Recycling*, 104:276–290, 2015.

[42] Die Hu, Baozhong Ma, Xiang Li, Yingwei Lv, Yongqiang Chen, and Chengyan Wang. Innovative and sustainable separation and recovery of valuable metals in spent cigs materials. *Journal of Cleaner Production*, 350:131426, 2022.

[43] R.R Maller. Passivation of stainless steel. *Trends in Food Science Technology*, 9(1):28–32, 1998.

[44] RS Lillard, GS Kanner, and DP Butt. The nature of oxide films on tungsten in acidic and alkaline solutions. *Journal of the Electrochemical Society*, 145(8):2718, 1998.

[45] Erik Lassner, Wolf-Dieter Schubert, Erik Lassner, and Wolf-Dieter Schubert. The element tungsten: Its properties. *Tungsten: Properties, Chemistry, Technology of the Element, Alloys, and Chemical Compounds*, pages 1–59, 1999.

[46] Ashish Pathak, Mari Vinoba, and Richa Kothari. Emerging role of organic acids in leaching of valuable metals from refinery-spent hydroprocessing catalysts, and potential techno-economic challenges: A review. *Critical Reviews in Environmental Science and Technology*, 51(1):1–43, 2021.

[47] U Jadhav, C Su, and H Hocheng. Leaching of metals from printed circuit board powder by an aspergillus niger culture supernatant and hydrogen peroxide. *RSC advances*, 6(49):43442–43452, 2016.

[48] Yang Qu, Bin Lian, Binbin Mo, and Congqiang Liu. Bioleaching of heavy metals from red mud using aspergillus niger. *Hydrometallurgy*, 136:71–77, 2013.

[49] Ignaz J Buerge and Stephan J Hug. Influence of organic ligands on chromium (vi) reduction by iron (ii). *Environmental science & technology*, 32(14):2092–2099, 1998.

[50] Cetin Kantar, Cihan Ari, and Selda Keskin. Comparison of different chelating agents to enhance reductive cr (vi) removal by pyrite treatment procedure. *Water research*, 76:66–75, 2015.

[51] Xiaolei Liu, Hailiang Dong, Xuewei Yang, Libor Kovarik, Yu Chen, and Qiang Zeng. Effects of citrate on hexavalent chromium reduction by structural fe (ii) in nontronite. *Journal of hazardous materials*, 343:245–254, 2018.

[52] Stephan J Hug, Hans-Ulrich Laubscher, and Bruce R James. Iron (iii) catalyzed photochemical reduction of chromium (vi) by oxalate and citrate in aqueous solutions. *Environmental science & technology*, 31(1):160–170, 1996.

[53] Megan Gaberell, Yu-Ping Chin, Stephan J Hug, and Barbara Sulzberger. Role of dissolved organic matter composition on the photoreduction of cr (vi) to cr (iii) in the presence of iron. *Environmental science & technology*, 37(19):4403–4409, 2003.

[54] Jun Sun, J-D Mao, Hui Gong, and Yeqing Lan. Fe (iii) photocatalytic reduction of cr (vi) by low-molecular-weight organic acids with α-oh. *Journal of hazardous materials*, 168(2-3):1569–1574, 2009.

[55] Fariborz Faraji, Amirhossein Alizadeh, Fereshteh Rashchi, and Navid Mostoufi. Kinetics of leaching: A review. *Reviews in Chemical Engineering*, 38(2):113–148, 2022.

[56] F Habashi. Kinetics of metallurgical processes, métallurgie extractive québec, québec city, canada 1999. distributed by laval university bookstore.

[57] Yubiao Li, N Kawashima, J Li, AP Chandra, and Andrea R Gerson. A review of the structure, and fundamental mechanisms and kinetics of the leaching of chalcopyrite. *Advances in colloid and interface science*, 197:1–32, 2013.

[58] Yuanhe Yue, Yuting Zhuo, Qiyuan Li, and Yansong Shen. Experimental and numerical study of extracting silver from end-of-life c-si photovoltaic solar cells in rotating systems. *Resources, Conservation and Recycling*, 186:106548, 2022.

[59] M. Marafi and E. Furimsky. Selection of organic agents for reclamation of metals from spent hydroprocessing catalysts. *Erdoel Erdgas Kohle*, 121:93–96, 02 2005.

[60] Jonas Schuster and Burçak Ebin. Investigation of indium and other valuable metals leaching from unground waste lcd screens by organic and inorganic acid leaching. *Separation and Purification Technology*, 279:119659, 2021.

A

Appendix 1

DEPARTMENT OF SOME SUBJECT OR TECHNOLOGY
CHALMERS UNIVERSITY OF TECHNOLOGY
Gothenburg, Sweden
www.chalmers.se

CHALMERS
UNIVERSITY OF TECHNOLOGY